18

Monte-Carlo Simulation of Ionizing Radiation Tracks

Ianik Plante and Francis A. Cucinotta
NASA Johnson Space Center, Houston, TX
USA

1. Introduction

Ionizing radiation comprises several types of energetic particles such as electrons, ions, and neutrons and energetic photons (X-rays or γ-rays). They are widely used in medicine for diagnosis and for cancer radiotherapy either as a curative or adjunctive treatments. Ionizing radiation is also known to increase cancer risk and other late risks include cataracts, heart disease and central nervous system effects. While the biological pathways involved in the effects of radiation are numerous and complex, they are initiated by physical, physico-chemical and chemical interactions of the radiation with the medium.

Because of the stochastic nature of radiation interactions, Monte-Carlo simulations techniques are very convenient not only to help our understanding of the mechanisms of interaction of ionizing radiation with matter, but they are also used in practical applications such as in microdosimetry, accelerator design and radiotherapy treatment planning. Therefore, several Monte-Carlo simulation codes of radiation tracks have been developed with different purposes (reviewed in Nikjoo et al., 2006).

In this chapter, the Monte-Carlo techniques used in particle transport related to energy deposition will be reviewed first. In the second part, the concept of *cross section* will be discussed. The cross sections are of particular importance for radiation transport, because they represent the probability of interaction of radiation with the medium. The *differential cross sections* are used to find the energy of the interaction and the direction of the particles afterward. The *total cross sections* are needed to calculate the mean free path between two interactions of the radiation. Therefore most of the discussion will be on the interaction cross sections for electrons, ions and photons, their sampling and their use in radiation transport codes.

2. Monte-Carlo techniques used in particle transport

Before discussing of the simulation of ionizing radiation tracks, some basic Monte-Carlo techniques used for particle transport will be introduced.

2.1 Random numbers

Monte Carlo simulations require large quantities of random numbers. A random number is defined as a particular value of a continuous random variable distributed uniformly in the interval [0,1]. The most commonly used type of random number generator is the so-called

congruential generator. A sequence of random numbers is generated from the integer number I_i by

$$I_{i+1} = (aI_i + c) \bmod (b) \tag{1}$$

where mod is the remainder of the division of aI_i+c by b. To obtain a number between 0 and 1, the result is divided by b: $R_i=I_i/b$. For example, setting a=7, c=3 and b=11 and an initial value I_i of 1 would give the sequence

$$1, 10, 7, 8, 4, 9, 0, 3, 2, 6, 1, 10,\ldots \tag{2}$$

An intial value of I_i, usually called *seed*, will always generate the same sequence of numbers. As illustrated in this example, this generator is not perfect since 5 is not in the sequence. The couple of successive points are also located along parallel lines on a 2D plot (sequential correlation), which would not be the case for a true random sequence. In fact, the algorithms used today fail statistic tests of randomness at some point (Devroye, 1986). Nevertheless, the congruential generator is widely use because of its simplicity and a period of ~10^9 when used with appropriate values of a,b and c (Press et al., 2000) which is sufficient for most purposes.

2.2 Sampling in a table

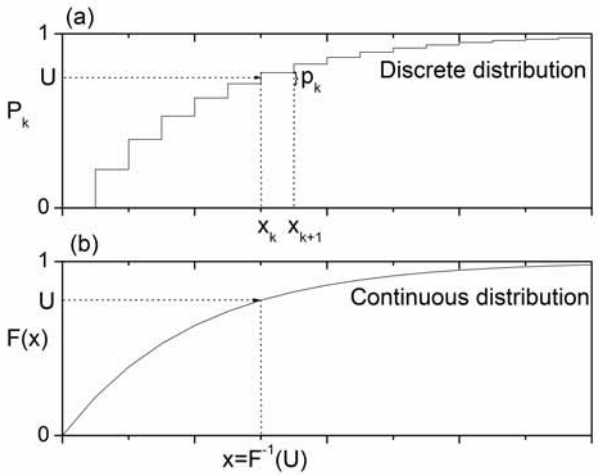


Fig. 1. Cumulative probability distributions for (a) a discrete distribution and (b) a continuous distribution.

In the theory of probability and statistics, a *probability distribution* is a function that maps events to real numbers (random variable). The distributions can be either discrete or continuous. A *discrete probability distribution* can only assume a finite or countably infinite random number of values. An example of this is the simulation of a toss of a dice. The N events for a dice are the numbers 1 to 6, each with $p_i=1/6$. The probabilities are normalized:

$$\sum_{i=1}^{N} p_i = 1 \tag{3}$$

The cumulative probabilities P_k are obtained by summing the p_i values from i=1 to i=k :

$$P_k = \sum_{i=1}^{k} p_i \tag{4}$$

Consider now the problem of obtaining computer generated random samples from uniform probability distributions. To simulate the toss of a dice, a random number in the interval [0,1] is drawn. Then the value of k which verifies $P_k < U \leq P_{k+1}$ is found as illustrated in Figure 1a. The random number U is placed on the left axis. The value of k is obtained by using the cumulative probability distribution. The value of k determines which event occurs.

2.3 Inversion method

In *continuous probability distributions*, the random variable can take an infinite number of possible values (for example, a position on the X axis). The probability to find a number between x and x+dx is described by the distribution f(x)dx. This distribution is normalized:

$$\int_{-\infty}^{\infty} f(x')dx' = 1 \tag{5}$$

The cumulative probability distribution F(x) is obtained by integration:

$$F(x) = \int_{-\infty}^{x} f(x')dx' \tag{6}$$

Let U be a random number uniformly distributed between 0 and 1 and X a random number distributed according to the density f(x). If F(x) is easy to obtain and invert, a value of X can be generated by invertion of the cumulative probability distribution:

$$F(X) = \int_{-\infty}^{X} f(x')dx' = U \tag{7a}$$

$$X = F^{-1}(U) \tag{7b}$$

The classical example to illustrate this method is the exponential distribution, which is also very important in particle transport. This distribution can be written:

$$f(x) = \lambda^{-1} \exp(-x/\lambda)\ ,\ x \geq 0,\ \lambda > 0 \tag{8}$$

The integration and inversion of the cumulative probability distribution gives:

$$X = -\lambda \log(1-U) \ \text{ or } \ X = -\lambda \log(U) \tag{9}$$

because 1-U is also an uniform distribution between 0 and 1. The inversion method is, as illustrated on Figure 1b, the continuous limit of sampling in a table.

2.4 Rejection method

It is not always be possible to apply the direct (or inversion) method of sampling. Another well established method is the so-called *rejection sampling* technique. The name comes from the fact that not all of the random samples generated are retained, some are rejected on the basis of a criterion which are now specified. Let f(x), the probability distribution to sample. Let further assume that f(x) can be written in the form

$$f(x) = g(x)\rho(x) \tag{10}$$

where g(x) is a probability distribution normalized and easy to sample such as the exponential and ρ(x) is a function bounded by a constant c≥1 (ρ(x)≤c). Random numbers distributed as f(x) can be generated by the following algorithm:

Algorithm 1: Rejection method
REPEAT
{
    Generate a random X distributed as g(x)
    Generate a uniform random number U (between 0 and 1)
}
UNTIL cU>ρ(X)
RETURN X ■

This method can be understood intuitively by looking at Figure 2. A point (X, cU) is generated in the plane. By selecting only the points which verifies the condition cU≤ρ(X), X is distributed as f(x).

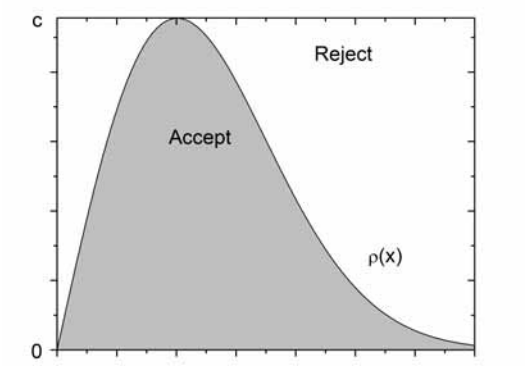


Fig. 2. Rejection method. A point (X,cU) is generated in the plane bounded by the constant c.

2.5 Composition method

The target density f(x) can sometimes be decomposed in a combination of probability distributions such as:

$$f(x) = \sum_{i=1}^{n} p_i g_i(x)\rho_i(x) \tag{11}$$

where the p_i form a probability vector (i.e. $p_i \geq 0$ for all i and $\Sigma p_i = 1$) and $\rho_i(x)$ are normalized probability distributions which can be sampled by inversion. Then the following algorithm may be used to generate X distributed as f(X):

Algorithm 2: Composition method
REPEAT
{
Generate uniform independent random numbers U_1, U_2 and U_3 (between 0 and 1)
Find the value of i for which $p_{i-1} < U_1 < p_i$
$X=\Theta_i^{-1}(U_2)$
}
UNTIL $U_3 > g_i(X)$
RETURN X ■

In this algorithm, $\Theta_i(x)$ is the cumulative probability distribution of $\rho_i(x)$. The random number U_1 determines which probability distribution is sampled. The distribution $\rho_i(x)$ is then generated by the rejection method described in the previous section.

3. Generalities in particle transport

The Monte-Carlo simulation of particle transport is basically following the trajectory of a particle in a medium and of all its interactions. A particle will be followed until it leaves the volume of interest, its energy decreases below a cutoff energy or disappears by a physical process (for example, a photon is absorbed by photoelectric effect). Of course, many other particles such as secondary electrons are generated and should also be followed. In this section, several important concepts used in particle transport for all radiation types are discussed: the direction vector, the cross sections and mean free path, the choice of an interaction and the change of direction following an interaction.

3.1 Coordinate system and direction vector

The particles used in radiation transport codes are usually attributed several characteristics such as an energy E, a position x,y,z and a direction given by θ and φ in a spherical coordinates system, which are the angles between the direction vector and the axis Oz and the azimutal angle in the plane Oxy. The direction vector is given by the direction cosines

$$\vec{v} = \begin{bmatrix} \sin(\theta)\cos(\varphi) \\ \sin(\theta)\sin(\varphi) \\ \cos(\theta) \end{bmatrix} \tag{12}$$

This coordinate system is shown on Figure 3.

3.2 Cross sections and mean free path

Let a flux of particles of intensity I and energy E interact with a layer of matter of density N and of width dx (Figure 4). After going through the layer, the intensity of the incident flux of particles is reduced by

$$dI = -\sigma(E)NIdx \tag{13}$$

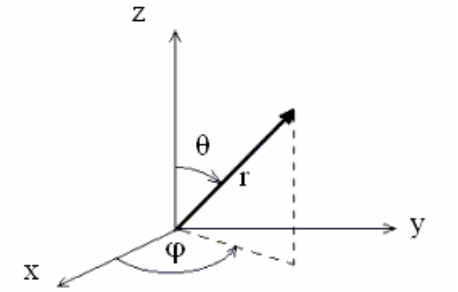


Fig. 3. Coordinate system in spherical coordinates. Here $0 \le \varphi \le 2\pi$ and $0 \le \theta \le \pi$.

Here, $\sigma(E)$ is the total interaction cross section by target atom (units: 1 barn=10^{-24} cm^2) or *microscopic cross section*. The *macroscopic cross section*, which is defined as $\Sigma(E)=N\sigma(E)$ (units: cm^{-1}), is also seen in some texts.

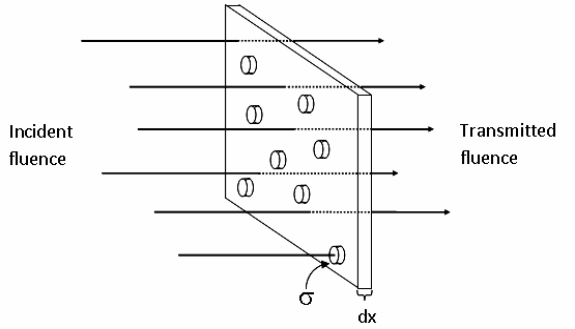


Fig. 4. Cross section. A layer of material of width dx is irradiated by an incident fluence of particles. The target molecules have a projected surface σ, representing their probability of interaction with the incident particles.

The cross section is assumed to be constant between two interactions. Hence equation (13) can be solved:

$$I(x) = I(0)\exp(-x / \lambda(E)) \tag{14}$$

Where $\lambda(E)=1/(N\sigma(E))$ is the mean free path (units : cm). Therefore the probability to find a particle which has not interacted at distance x from its original position is distributed exponentially. In particle transport codes, a distance s between two interactions is usually sampled by using the inversion method for the exponential distribution:

$$s = -\lambda \log(U) \tag{15}$$

Therefore, the next interaction of the particle will be at the position (x′,y′,z′):

$$\begin{aligned} x' &= x + s\sin(\theta)\cos(\varphi) \\ y' &= y + s\sin(\theta)\sin(\varphi) \\ z' &= z + s\cos(\theta) \end{aligned} \tag{16}$$

We conclude this section by mentioning that the cross sections discussed yet are the *total cross sections*. They are often found by integrating the *differential cross section* in angle and/or in energy.

3.3 Choice of interaction

In general, the total interaction cross section is the sum of several interaction cross sections. The total cross section is used to find the distance between two interactions. The ratio between the cross section for a given type of interaction to the total cross section represents the probability for a type of interaction to occur. Therefore, the sampling in a table technique may be used to determine the type of interaction. Of course, since a particle loses energy at each inelastic interaction, the cross sections should be updated at each timestep.

3.4 Change of direction following an interaction

After an interaction, the direction of the trajectory of a particle change. Let the direction of the trajectories before and after the interaction described by the vectors $\vec{v}_0$ and $\vec{v}_1$:

$$\vec{v}_0 = \begin{bmatrix} v_{0_x} \\ v_{0_y} \\ v_{0_z} \end{bmatrix} = \begin{bmatrix} \sin(\theta_0)\cos(\varphi_0) \\ \sin(\theta_0)\sin(\varphi_0) \\ \cos(\theta_0) \end{bmatrix}; \vec{v}_1 = \begin{bmatrix} v_{1_x} \\ v_{1_y} \\ v_{1_z} \end{bmatrix} = \begin{bmatrix} \sin(\theta_1)\cos(\varphi_1) \\ \sin(\theta_1)\sin(\varphi_1) \\ \cos(\theta_1) \end{bmatrix} \tag{17}$$

The angles θ_0, φ_0, θ_1 and φ_1 are the angles of the trajectory of the particle in the laboratory frame in spherical coordinates (Figure 3). We also define

$$A_{1,0} = \sin(\theta_0)\cos(\varphi_0) \tag{18a}$$

$$A_{2,0} = \sin(\theta_0)\sin(\varphi_0) \tag{18b}$$

Following an interaction from which the trajectory is deflected by the angles θ and φ relatively to the initial trajectory, the new trajectory of the particle $\vec{v}_1$ should be found in the laboratory frame (R). To do so, a rotation to a reference frame (R'') in which $\vec{v}_0$ is oriented along the z'' axis is performed. Therefore a transformation to go from the referential R'' to R and its inverse is needed. The transformation R→R'' is as follows:

1. A rotation of φ_0 around the z axis to bring $\vec{v}_0$ in the plane Ox'z'.
2. A rotation of θ_0 around the y' axis to bring $\vec{v}_0$ in the direction z''

These transformations can be written by using the (inverse) rotation matrix:

$$\vec{v}_0' = \begin{bmatrix} v_{0_x}' \\ v_{0_y}' \\ v_{0_z}' \end{bmatrix} = \begin{bmatrix} \cos(\theta_0) & 0 & \sin(\theta_0) \\ 0 & 1 & 0 \\ -\sin(\theta_0) & 0 & \cos(\theta_0) \end{bmatrix} \begin{bmatrix} v_{0_x}'' \\ v_{0_y}'' \\ v_{0_z}'' \end{bmatrix} = \begin{bmatrix} v_{0_x}'' \cos(\theta_0) + v_{0_z}'' \sin(\theta_0) \\ v_{0_y}'' \\ -v_{0_x}'' \sin(\theta_0) + v_{0_z}'' \cos(\theta_0) \end{bmatrix} \tag{19a}$$

$$\vec{v}_0 = \begin{bmatrix} v_{0_x} \\ v_{0_y} \\ v_{0_z} \end{bmatrix} = \begin{bmatrix} \cos(-\varphi_0) & \sin(-\varphi_0) & 0 \\ -\sin(-\varphi_0) & \cos(-\varphi_0) & 0 \\ 0 & 0 & 1 \end{bmatrix} \begin{bmatrix} v_{0_x}' \\ v_{0_y}' \\ v_{0_z}' \end{bmatrix} = \begin{bmatrix} v_{0_x}' \cos(\varphi_0) - v_{0_y}' \sin(\varphi_0) \\ v_{0_x}' \sin(\varphi_0) + v_{0_y}' \cos(\varphi_0) \\ v_{0_z}' \end{bmatrix} \tag{19b}$$

Combining these equations gives

$$\vec{v}_0 = \begin{bmatrix} v_{0_x} \\ v_{0_y} \\ v_{0_z} \end{bmatrix} = \begin{bmatrix} (v''_{0_x}\cos(\theta_0) + v''_{0_z}\sin(\theta_0))\cos(\varphi_0) - v''_{0_y}\sin(\varphi_0) \\ (v''_{0_x}\cos(\theta_0) + v''_{0_z}\sin(\theta_0))\sin(\varphi_0) + v''_{0_y}\cos(\varphi_0) \\ -v''_{0_x}\sin(\theta_0) + v''_{0_z}\cos(\theta_0) \end{bmatrix} \tag{20}$$

In the R'' system, the direction vector after the interaction is given by

$$\vec{v}''_1 = \begin{bmatrix} v''_{1_x} \\ v''_{1_y} \\ v''_{1_z} \end{bmatrix} = \begin{bmatrix} \sin(\theta)\cos(\varphi) \\ \sin(\theta)\sin(\varphi) \\ \cos(\theta) \end{bmatrix} \tag{21}$$

To calculate $\vec{v}_1$ in the laboratory frame, the transformation R''→R is applied. After some calculations, we find

$$\cos(\theta_1) = \cos(\theta)\cos(\theta_0) - \sin(\theta)\cos(\varphi)\sin(\theta_0) \tag{22a}$$

$$\cos(\varphi_1) = \frac{1}{\sin(\theta_1)}\left[(\sin(\theta)\cos(\varphi)\cos(\theta_0) + \cos(\theta)\sin(\theta_0))\cos(\varphi_0) - \sin(\theta)\sin(\varphi)\sin(\varphi_0)\right] \tag{22b}$$

$$\sin(\varphi_1) = \frac{1}{\sin(\theta_1)}\left[(\sin(\theta)\cos(\varphi)\cos(\theta_0) + \cos(\theta)\sin(\theta_0))\sin(\varphi_0) + \sin(\theta)\sin(\varphi)\cos(\varphi_0)\right] \tag{22c}$$

This gives the algorithm for the change of direction. $A_{1,0}$, $A_{2,0}$, A_3, A_4 and A_5 are calculated first:

$$A_{1,0} = \sin(\theta_0)\cos(\varphi_0) \tag{23a}$$

$$A_{2,0} = \sin(\theta_0)\sin(\varphi_0) \tag{23b}$$

$$A_3 = \sin(\theta)\cos(\varphi) \tag{23c}$$

$$A_4 = A_3\cos(\theta_0) + \cos(\theta)\sin(\theta_0) \tag{23d}$$

$$A_5 = \sin(\theta)\sin(\varphi) \tag{23e}$$

After the interaction, A_1 and A_2 becomes

$$A_{1,1} = A_4\cos(\varphi_0) - A_5\sin(\varphi_0) \tag{24a}$$

$$A_{2,1} = A_4\sin(\phi_0) + A_5\cos(\phi_0) \tag{24b}$$

The angles θ_1 and φ_1 can now be calculated in the laboratory frame:

$$\cos(\theta_1) = \cos(\theta_0)\cos(\theta) - A_3 \sin(\theta_0) \tag{25a}$$

$$\sin(\theta_1) = \sqrt{1 - \cos^2(\theta_1)} \tag{25b}$$

$$\cos(\varphi_1) = A_{1,1} / \sin(\theta_1) \tag{25c}$$

$$\sin(\varphi_1) = A_{2,1} / \sin(\theta_1) \tag{25d}$$

4. Simulation of ionizing radiation tracks

The energy deposition by radiations is strongly dependent on the type and energy of radiation. Most damage induced by radiation to biomolecules leading to biological consequences are not caused by the direct impact of the primary radiation but are induced by secondary electrons and chemical species generated by the primary ionizing particle (O'Neill & Wardman, 2009). In fact, secondary electrons are produced in large quantities by the attenuation of all energetic primary ionizing radiations such as β- and α-particles, heavy ions, X-rays and γ-rays (Pimblott & LaVerne, 2007). These secondary electrons also cause additional ionization and excitations in the medium, leading to the formation of radiation chemical spurs[1] (Mozumder & Magee, 1966). Therefore the simulation of electron tracks is a very important subject, which is part of every radiation transport code. In this section, the cross sections used in the code RITRACKS (Plante & Cucinotta, 2008; 2009) are shown. The cross sections used in RITRACKS are relativistic, but the discussion will be limited here to the non-relativistic energy range. Moreover, since the sampling of the cross sections for electrons and ions was discussed in (Plante & Cucinotta, 2008; 2009), only the sampling of the cross sections for photons will be detailed here.

4.1 Electrons

A large portion of the secondary electrons created by ionizing radiation have low energy (<100 eV) (Pimblott & LaVerne, 2007). These electrons are very important since they have been shown to create irreversible damage to DNA and other molecules as well (Boudaïffa et al, 2000). Some secondary electrons may have energies in the MeV region depending on the initial radiation type and energy. These electrons can travel several millimeters in biological media (Meesungnoen et al., 2002) and affect cells far away from the trajectory of the radiation track. Electrons interact with matter by ionizations, excitations, elastic collisions and dissociative attachment.

4.1.1 Ionization

Ionization is the most important process for energy loss by electrons >10 eV. The molecular orbitals of water are $^1b_1$, $^3a_1$, $^1b_2$, $^2a_1$ and $^1a_1$. A convenient expression for the cross sections is given by the Rudd's semi-empirical equation (Rudd, 1990):

$$\frac{d\sigma_{ion}^{i}}{dw} = \frac{d\sigma_{ion}^{i(1)}}{dw} + \frac{d\sigma_{ion}^{i(2)}}{dw} \tag{26a}$$

[1] A *spur* is a cluster of chemical species produced by the radiolysis of water

$$\frac{d\sigma_{ion}^{i(1)}}{dw} = \frac{S_i}{I_i} F_1(t) \left[\frac{1}{(1+w)^3} + \frac{1}{(t-w)^3} - \frac{1}{(1+w)^{3/2}(t-w)^{3/2}} \right] \tag{26b}$$

$$\frac{d\sigma_{ion}^{i(2)}}{dw} = \frac{S_i}{I_i} F_2(t) \left[\frac{1}{(1+w)^2} + \frac{1}{(t-w)^2} - \frac{1}{(1+w)(t-w)} \right] \tag{26c}$$

The differential cross section is written as a function of $t=T/I_i$ and $w=W/I_i$, where T is the energy of the primary electron, W is the energy of the ionized electron and I_i is the binding energy of the molecular orbital. The multiplicative factor $S_i = 4\pi a_0^2 N_i (\Re / I_i)^2$, a_0 is Bohr's radius (5.3×10^{-11} m), $\Re$ is Rydberg energy (13.6 eV) and N_i is the number of electrons in the orbital, which is 2 in every case. The functions $F_1(t)$ and $F_2(t)$ are given by:

$$F_1(t) = A_1 \frac{\ln(t)}{t + B_1} \; ; F_2(t) = \frac{A_2}{t + B_2} \tag{27}$$

The parameters A_1, A_2, B_1 and B_2 (Table 1) were determined by fitting experimental data.

Parameter	External shells	Internal shells
A_1	0.94	1.31
A_2	1.13	0.37
B_1	2.30	0.00
B_2	22.0	0.00

Table 1. Parameters used in Rudd's equation for electrons

The total cross section is calculated by integrating the differential cross section over W:

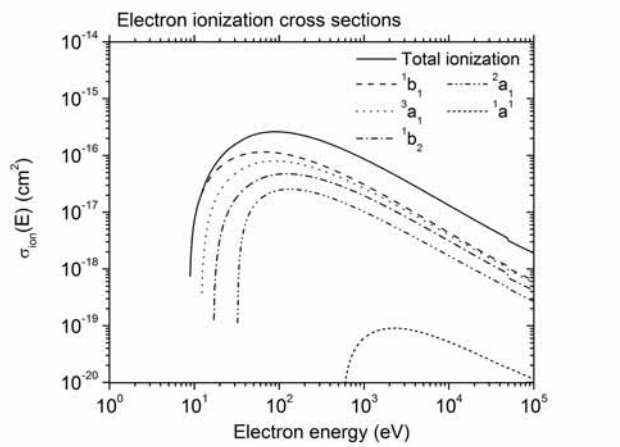
$$\sigma_{ion}^{i} = \int_0^{E_{max}+I_i} \frac{d\sigma_{ion}^{i}}{dW} dW \tag{28}$$

This integral can be evaluated analytically. The maximum energy transfer (E_{max}) for classical or relativistic electrons it T/2, because the incident and secondary electron are indiscernable. Replacing E_{max} by T/2, the result of the integral can be written:

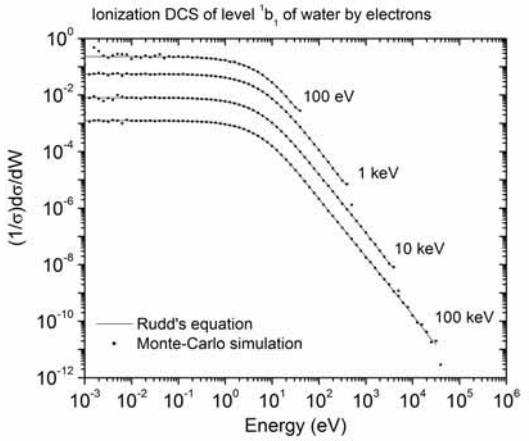
$$\sigma_{ion}^{i} = S_i F_1(t) \frac{t-1}{2t^2} \left(t + 1 - \frac{4\sqrt{t}}{3+t} \right) + S_i F_2(t) \left(1 - \frac{1}{t} - \frac{\ln(t)}{t+1} \right) \tag{29}$$

The ionization cross sections by electron for each orbital are shown on Figure 5. The differential cross section for the ionization of the orbital $^1b_1$ of water by 0.1, 1, 10 and 100 keV electrons is obtained by sampling in a table.

The orbital $^1a_1$ is an internal orbital of the water molecule. The ionization of this orbital is much less frequent than ionization of external shells. The vacancy created result in a reorganization of the molecule, leading to the emission of an Auger electron. Finally, Rudd's equation does not applies to electrons with relativistic energies (>150 keV). In this case, Seltzer's equation may be used (Uehara et al., 1992; Nikjoo et al., 2008; Plante and Cucinotta, 2009).



(a)



(b)

Fig. 5. a) Total electron ionization cross section for water calculated by Rudd's formula for energy <50 keV for excitation levels $^1b_1$, $^3a_1$, $^1b_2$, $^2a_1$ et $^1a_1$. b) Energy distribution of ionized electrons calculated by Rudd's formula for 10^2, 10^3, 10^4 and 10^5 eV incident electrons for the molecular orbital $^1b_1$ of water.

4.1.2 Excitations

Excitation cross sections are about an order of magnitude lower than the ionization cross sections, except at low energy. The relative contribution of the excited states $\tilde{A}^1B_1$, $\tilde{B}^1A_1$, Rydberg series A+B and C+D, diffuse band and plasmon (collective) excitation is controversial (Dingfelder et al., 1999; Nikjoo et al., 2006). In RITRACKS, only the states $\tilde{A}^1B_1$, $\tilde{B}^1A_1$ and plasmon excitation are included (Cobut et al., 1998).

A model of differential cross section for the energy loss W by excitation in liquid water was proposed by Kutcher & Green (1976):

$$\frac{d\sigma_{ex}^{i}}{dW} = \rho(W) W f_i(W) \ln\left[\frac{\alpha(T) T}{W}\right] \tag{30}$$

Here, T is the energy of the incident electron, ρ(W) is the differential cross section for charged particles interacting with electron at rest and $f_i(W)$ are functions to be defined later. The parameter α(T) was introduced by Cobut (1993) to link the cross sections at high and low energy. The cross section ρ(W) is given by

$$\rho(W) = \frac{e^4}{8\pi\varepsilon_0^2 m v^2 W^2} = \frac{4\pi a_0^2}{T}\left(\frac{\Re}{W}\right)^2 \tag{31}$$

In this equation, a_0 is Bohr's radius, ε_0 is vacuum permittivity, ℜ is Rydberg energy and m, v and e are the mass, velocity and charge of the electron. The parameter α(T) is given by

$$\alpha(T) = 4 - 3\exp[-(W - W_{0,i}) / \alpha_i] \tag{32}$$

where $\alpha_j = E_{min}(\beta^* - 1)/\ln(2)$, β^*=5 and E_{min}=7.34 eV (Cobut et al., 1998). When $T \to W_{0,i}$, $\alpha(T) \to 1$; when $T \to \infty$, $\alpha(T) \to 4$. This parameter varies slowly between 1 and 4. The functions $f_i(W)$ for the excitation levels $\tilde{A}^1B_1$ and $\tilde{B}^1A_1$ are Gaussian:

$$f_i(W) = f_{o,i}\sqrt{\frac{\alpha_i}{\pi}} \exp\left[-\alpha_i (W - W_{0,i})^2\right] \tag{33}$$

For plasmon excitation, $f_i(W)$ is given by:

$$f_i(W) = f_{o,pl}\alpha_{pl} \frac{e^\tau}{(1 + e^\tau)^2} \tag{34}$$

where $\tau = \alpha_{pl}(W - W_0)$. The parameters $f_{0,i}$, α_i et $W_{0,i}$ are given in table 2.

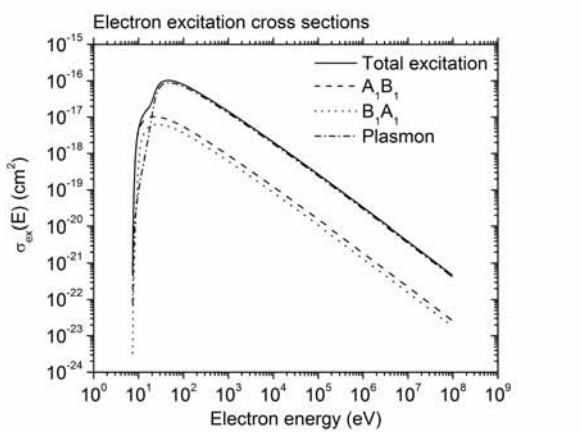
	$\tilde{A}^1B_1$	$\tilde{B}^1A_1$	Plasmon
f_{0i}	0.0187	0.0157	0.7843
α_i	3 (eV^{-2})	1 (eV^{-2})	0.6 (eV^{-1})
W_{0i} (eV)	8.4	10.1	21.3

Table 2. Parameters used to calculate the functions $f_i(W)$

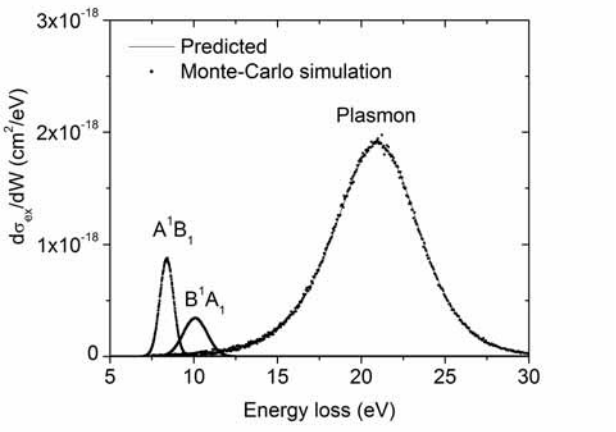
The excitation cross section for the excitation level i is calculated by integrating numerically the differential cross section:

$$\sigma_{ex}^{i} = \int_{7.34}^{\min(100,T)} \rho(W) W f_i(W) \ln\left[\frac{\alpha(T) T}{W}\right] dW \tag{35}$$

The inferior limit of integration is 7.34 eV, which is the minimal energy transferred by excitation. The superior limit is the lowest value between 100 eV and the energy of the incident electron. These limits covers the domain where the functions $f_i(W)$ are significant, which are very narrow peaks between [7.18, 9.63] and [7.98,12.2] eV for the levels $\tilde{A}^1B_1$ and $\tilde{B}^1A_1$ and between [12.5-30.1] eV for plasmon excitation.



(a)



(b)

Fig. 6. a) Excitation cross sections for levels $\tilde{A}^1B_1$, $\tilde{B}^1A_1$ and plasmon excitation. Right: DCS of the energy loss of 1 MeV electron by excitation for levels $\tilde{A}^1B_1$, $\tilde{B}^1A_1$ and plasmon excitation in liquid water. The area is proportional to the cross section. b) Sampling of the energy loss by a 1 keV electron by excitation.

4.1.3 Excitation of vibration and rotation levels

Experiments by Michaud et al. (2003) for 1-100 eV electrons have shown that it is possible to excite vibration and rotation levels of water molecules. Contrary to the excitation described in the previous section, they do not lead to the dissociation of the water molecule. These cross sections have been included in the code RITRACKS. Several vibration and rotation level exists, but they will not be detailed here (See Michaud et al., 2003).

4.1.4 Dissociative electron attachment

Attachment of an electron with a water molecule leads to the following sequence of events:

$$H_2O + e^- \rightarrow H_2O^- \rightarrow H^- + {}^{\bullet}OH \tag{36}$$

This process is the dissociative attachment. In water, H^- is very unstable and reacts with a neighbor water molecule to give non-captable molecular hydrogen (Jay-Gerin & Ferradini, 1999).

$$H^- + H_2O \rightarrow H_2 + OH^- \tag{37}$$

The dissociative attachment has been observed experimentally (Rowntree et al., 1991). It happens only at low energy (~6-7 eV).

4.1.5 Elastic collisions

During an elastic collision, there is no loss of energy by the electron. Therefore, only the deflection angle should be determined when an elastic collision occurs.

Electrons of energy below 200 eV

For energies below 200 eV, the experimental elastic cross section of Michaud et al. (2003) is used. When an elastic scattering event occurs, the semi-empirical DCS parameterized by Brenner & Zaider (1983) is used to sample the angle of deflection. It can be written as:

$$\frac{d\sigma_{el}}{d\Omega} = \alpha(T)\left\{\frac{1}{\left[1 + 2\gamma(T) - \cos(\theta)\right]^2} + \frac{\beta(T)}{\left[1 + 2\delta(T) + \cos(\theta)\right]^2}\right\} \tag{38}$$

where T is the energy of the electron, $\alpha(T)$ is a proportionality constant, $\beta(T)$, $\gamma(T)$ and $\delta(T)$ are parametric functions in the form of exponentials and polynomials, θ is the angle of deflection and $d\Omega=2\pi\sin(\theta)d\theta$ is the differential solid angle element in the direction θ.

Electrons of energies over 200 eV

For electrons with energies over 200 eV, the Rutherford cross section with a screening parameter η (Uehara et al., 1992) are used in RITRACKS:

$$\frac{d\sigma_{el}}{d\Omega} = \frac{Z(Z+1)r_e^2}{\left(1 - \cos(\theta) + 2\eta\right)^2}\frac{1-\beta^2}{\beta^4} \tag{39}$$

Here, r_e is the classical electron radius and β is the relativistic velocity (v/c). This equation is relativistic and can be used at high energies. The screening parameter η depends of the atomic number (Z) of the target.

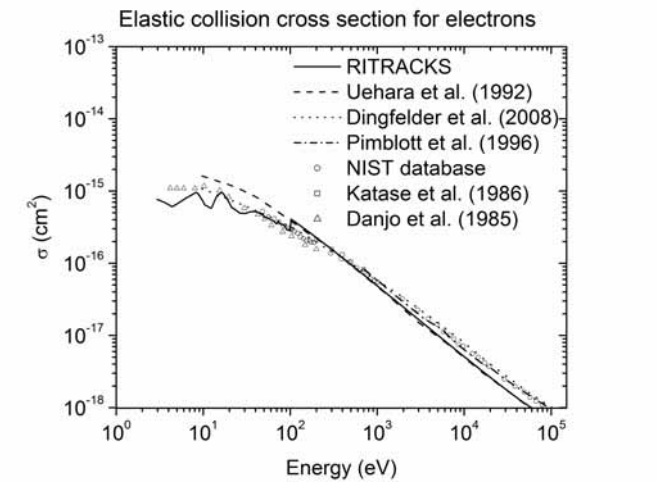
$$\eta = \eta_c \frac{1.7x10^{-5}Z^{2/3}}{\tau(\tau+2)} \tag{40}$$

Integration over $d\Omega$ yields the total elastic cross section:

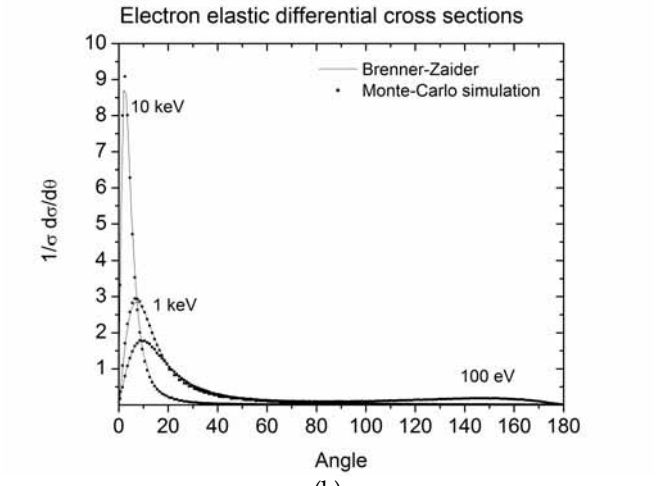
$$\sigma_{el} = \int_0^{\pi} 2\pi \frac{d\sigma_{el}}{d\Omega}\sin(\theta)d\theta = \frac{\pi Z(Z+1)r_e^2}{\eta(\eta+1)}\frac{1-\beta^2}{\beta^4} \tag{41}$$

For a molecular target like water, an effective value Z_{eff} is used instead of Z. The values proposed by Uehara et al. (1992) have been tried to join the experimental results at 200 eV.

The value Z_{eff}=7.22 have been chosen. The total elastic cross section used in RITRACKS is shown on Figure 7 and compared with calculations (Dingfelder et al., 2008; Uehara et al., 1992; Pimblott et al., 1996) and experimental data (Powell et al., 2005; Katase et al., 1986; Danjo & Nishimura, 1985).



(a)



(b)

Fig. 7. a) Elastic cross sections. The cross section from Michaud et al. (2003) are used for energies < 100 eV. For energies > 100 eV, the Rutherford cross section with the screening parameter η (see text) is used. The elastic cross section used by Dingfelder et al. (2008), Uehara et al. (1992) and Pimblott et al. (1996) are also shown. Experimental data: NIST Database (Powell et al., 2005), Katase et al. (1986) and Danjo & Nishimura (1985). b) Elastic DCS calculated with the parameterization of Brenner & Zaider (1983). The lines are the analytical models; the small dots are obtained by sampling the DCS.

4.2 Ions

Heavy ions of all charges from proton to uranium are present in space, the great majority being protons and α-particles. Their energies cover a large spectrum extending from a few MeV/nucleon to nearly 10^{15} MeV/nucleon, with a peak at ~1 GeV/amu. Heavy ions are shielded by the Earth's magnetosphere and atmosphere. In space, however, high charged (Z) and energy (HZE) particles such as $^{56}Fe^{26+}$ are very penetrating and may collide with nuclei of the atoms they encounter, fragmenting either the target and/or the projectile, which produces several secondary particles. Therefore it impossible to completely shield astronauts from these radiations and they are of concern for a long term space mission such as the 3-years Mars mission which would lead to whole-body dose of about 1 Sievert (Sv) or more. On travelling to Mars, it is estimated that every cell nucleus in an astronaut's body would be hit by a proton or secondary electron (eg, electrons of the target atoms ionized by the HZE ion) every few days and by an HZE ion about once a month (Cucinotta & Durante, 2006). Energy deposition by HZE ions is highly heterogeneous, with a localized contribution along the trajectory of every particle and lateral diffusion of energetic electrons (i.e. δ-rays, the target atom electrons ionized by the incident HZE ion and emitted at high energy) many microns from the path of the ions. These particles are therefore densely ionizing along the primary track (e.g. the track followed by the incident heavy ion, the so-called *core*); moreover, they are surrounded by a region (*penumbra*) comprising the high-energy electrons ejected by ions. As heavy ions slow down, they lose a larger part of their energy. Before they stop, heavy ions deposit a high fraction of their energy in a small region, named the *Bragg peak*. Therefore, heavy ions are gaining importance in radiotherapy, because of their advantageous dose profile which allows the deposition a larger amount of dose to the tumor and sparing of normal tissue.

4.2.1 Ionization

Rudd (1990) have also proposed a semi-empirical equation for the differential ionization cross sections of the molecular orbitals $^1b_1$, $^3a_1$, $^1b_2$, $^2a_1$ et $^1a_1$ of liquid water by protons:

$$\frac{d\sigma_{ion}^{i}}{dw} = \frac{S_i}{I_i} \frac{F_1(v) + wF_2(v)}{(1+w)^3 \left\{1 + \exp[\alpha(w - w_{c_i}) / v]\right\}} \tag{42}$$

As for electrons, i is the index of the orbital, I_i is the binding energy, $w=W/I_i$, W is the secondary electron energy and $S_i = 4\pi a_0^2 N_i \left(\Re / I_i\right)^2$. Furthermore, $T=E_p(m/M_p)$, M_p and E_p are the mass and energy of the incident proton, m is the electron mass, and $v=\sqrt{T / I_i}$ and $w_c = 4v^2 - 2v - \Re / 4I_i$. The functions $F_1(v)$ and $F_2(v)$ are defined as:

$$F_1(v) = L_1 + H_1 \; ; \; F_2(v) = \frac{L_2 H_2}{L_2 + H_2} \tag{43}$$

where

$$L_1 = \frac{C_1 v^{D_1}}{1 + E_1 v^{D_1+4}} \; ; \; H_1 = \frac{A_1 \ln(1+v^2)}{v^2 + B_1 / v^2} \tag{44a}$$

$$L_2(v) = C_2 v^{D_2} \; ; \; H_2 = A_2 / v^2 + B_2 / v^4 \tag{44b}$$

The parameters A_1,B_1…B_2..D_2 and α were determined by fitting experimental data (Table 1).

Parameter	External orbitals	Internal orbitals	Parameter	External orbitals	Internal orbitals
A_1	0.97	1.25	A_2	1.04	1.10
B_1	82.0	0.50	B_2	17.3	1.30
C_1	0.40	1.00	C_2	0.76	1.00
D_1	-0.30	1.00	D_2	0.04	0.00
E_1	0.38	3.00	α	0.64	0.66

Table 4. Parameters used in Rudd's equation for protons

The total ionization cross section is found by numerically integrating

$$\sigma_{ion}^{i} = \int_{0}^{E_{max}+I_i} \frac{d\sigma_{ion}^{i}}{dW} dW \tag{45}$$

Here, E_{max} is the maximal energy transfer in a single collision. In classical mechanics, this energy is given for an ion of mass M and energy E by (Turner, 2007):

$$E_{max} = \frac{4mME}{(M+m)^2} \cong 4\frac{m}{M}E \tag{46}$$

The total ionization cross section for the molecular orbitals $^1b_1$, $^3a_1$, $^1b_2$, $^2a_1$ and of water and the differential cross section for ionization of orbital $^1b_1$ by protons are shown on Figure 8.

4.2.2 Excitations

The excitation cross section is about one order of magnitude lower than the ionization cross section at a given energy. As for electrons, the relative contributions of each discrete electronic excitation levels so-called $\tilde{A}^1B_1$, $\tilde{B}^1A_1$, Ryd A+B, Ryd C+D (Rydberg series), diffuse bands and plasmon excitation (collective excitation) is currently debated (Nikjoo et al., 2006). The expression of these discrete excitation levels can be calculated by using the semi-empirical formulation shown in Dingfelder et al. (2006) or in Kutcher and Green (1976). In the former, for reasons that are discussed in Cobut et al. (1998), only the excitation levels $\tilde{A}^1B_1$, $\tilde{B}^1A_1$, and plasmon are considered. The differential cross section can also be written with the semi-empirical equation of Kutcher and Green (1976):

$$\frac{d\sigma_{ex}^{i}}{dW} = \rho(W) W f_i(W) \ln\left(\frac{4T}{W}\right) \tag{47}$$

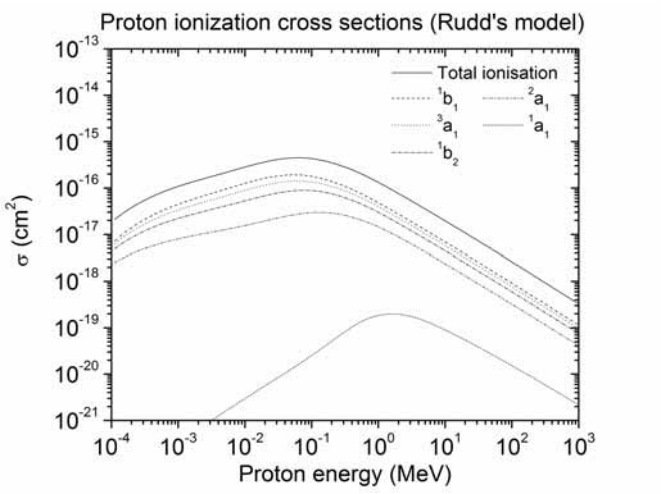
where

$$\rho(W) = \frac{Z^2 e^4}{8\pi\varepsilon_0^2 m v^2 W^2} = \frac{4\pi a_0^2 Z^2}{T}\left(\frac{\Re}{W}\right)^2 \tag{48}$$

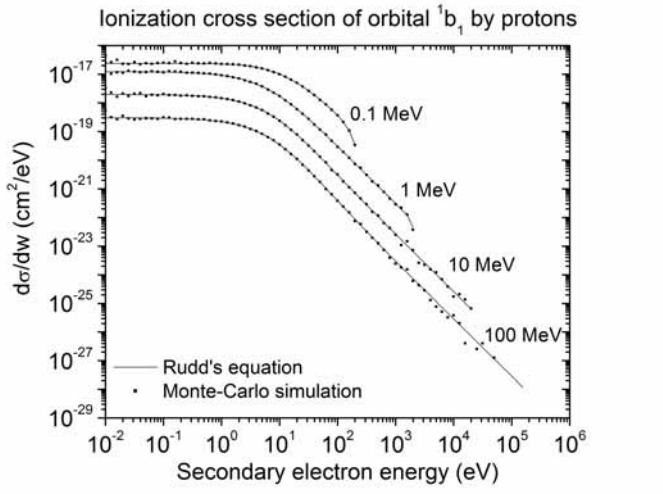
Here, W is the energy loss by excitation, $\rho(W)$ is the differential cross section for charged particle scattering on free electrons at rest, T=E(m/M), a_0 is the Bohr radius, ε_0 is vaccuum permittivity, m is electron mass and M, E, v and Z are the mass, energy, velocity and charge of the incident ion. Note that the definition of W and v are different from the previous section. The functions $f_i(W)$ are the same as those defined previously for electrons. The total excitation cross section is calculated by integrating numerically equation (47):

$$\sigma_{ex}^{i} = \int_{0.01}^{100} \rho(W) W f_i(W) \ln\left[\frac{4T}{W}\right] dW \tag{49}$$

The integration limits used here are empirical; as for electrons, they are chosen to cover the domain for which the functions $f_i(W)$ are significant. These cross sections are shown on Figure 9.

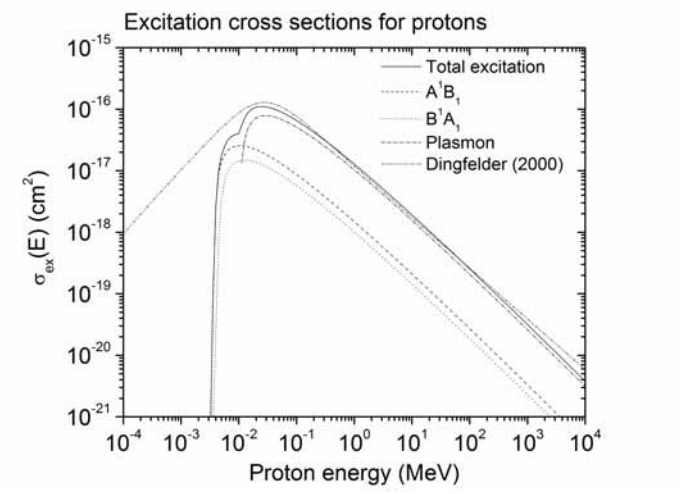


(a)

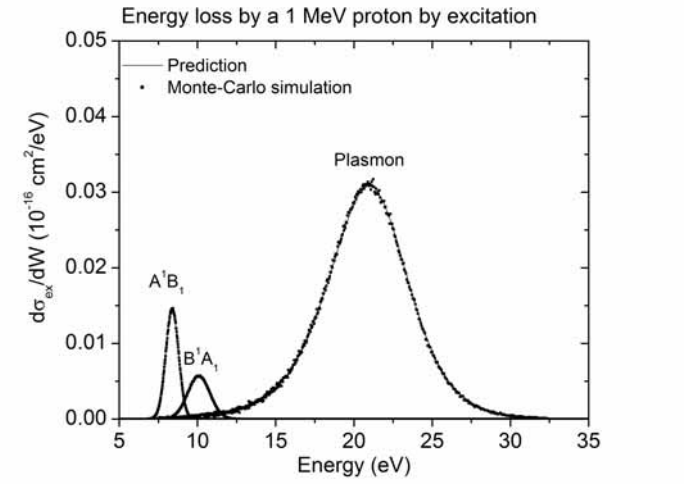


(b)

Fig. 8. a) Ionization cross sections for ionization of the molecular orbitals $^1b_1$, $^3a_1$, $^1b_2$, $^2a_1$ and $^1a_1$ of liquid water by protons. b) Sampling of the differential ionization cross section of the orbital $^1b_1$ by protons of 0.1, 1, 10 and 100 MeV and comparison with Rudd's equation.



(a)



(b)

Fig. 9. a) Excitation cross sections for levels $\tilde{A}^1B_1$, $\tilde{B}^1A_1$ and plasmon excitation of water molecule by protons. b) DCS of the energy loss of 1 MeV proton by excitation for levels $\tilde{A}^1B_1$, $\tilde{B}^1A_1$ and plasmon in liquid water. The area is proportional to the cross section.

4.2.3 Heavy ions cross sections

A heavy ion of mass M_{ion} with kinetic energy $E_{ion} = (M_{ion} / m_p)E_p$ has the same velocity of a proton (mass m_p) with kinetic energy E_p. This is true for both non-relativistic and relativistic ions (Dingfelder, 2006). Therefore, within the first order plane wave Born approximation, the interaction cross section for bare heavy ions of velocity v are obtained from proton interaction cross sections by scaling the differential cross section for a proton with the same velocity v by the square of the charge Z_0 of the ion (Dingfelder et al., 2006):

$$\frac{d\sigma_{ion}(v)}{dW} = Z^2 \frac{d\sigma_{proton}(v)}{dW} \tag{50}$$

Heavy ions at small energies have electrons attached and thus have a reduced charge $Z_{eff}<Z$. If Z_{eff} is defined to give the correct observed stopping power, it is not equal to the mean charge per particle of a beam leaving an absorber (Tai et al., 1997). An equation from Barkas (1963) is commonly used for the effective charge:

$$Z_{eff} = Z[1 - \exp(-125\beta Z^{-2/3})] \tag{51}$$

4.3 Photons

Photons such as γ-rays or X-rays have been used for decades in radiotherapy and are still widely used today. Over last years, several techniques such as stereotactic radiosurgery, 3D conformal radiotherapy (3DCRT) and Intensity-Modulated Radiation Therapy (IMRT) have evolved to deliver radiotherapy more efficiently and reducing secondary effects (Reynaert et al., 2007).

In the energy range between 100 eV to 2 MeV, photons interact with medium mainly by Compton effect, which results in the emission of a Compton electron and a photon with smaller energy. Photons of low energy are usually absorbed by photoelectric effect, resulting in the emission of a photoelectron. Therefore, photons also lead to production of electrons in the medium. Pair production (creation of an electron and a positron) can also occur, but only at energies greater than 1.022 MeV. Since the probability of pair production is small in the energy range under consideration, it will be neglected in this discussion. The photonuclear reactions are also neglected because the energy threshold for these reactions is above a few MeV and their cross section is relatively small (Anderson, 1984). For this work, the absorption coefficients given by Storm & Israel (1967) are used (figure 10).

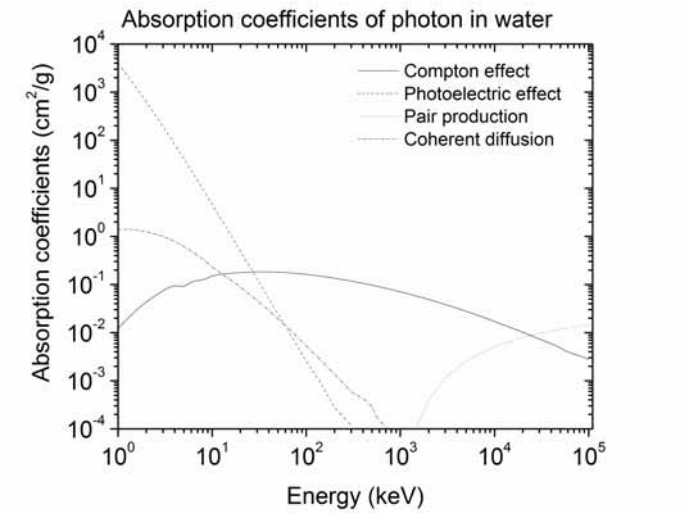


Fig. 10. Absorption coefficients for Compton effect, photoelectric effect, pair production and coherent diffusion for photons in water.

4.3.1 Compton effect

The Compton effect is the interaction of a photon with an electron. The initial photon has an energy hν. A part of this energy is transferred to the electron and a new photon of energy hν′ is scattered. For this work, the notation of Davisson & Evans (1952) is used.

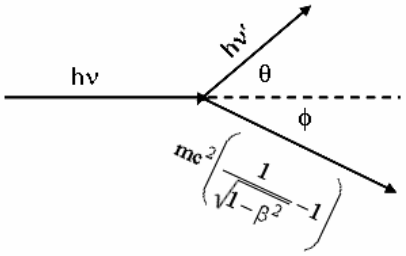


Fig. 11. Compton effect. A photon with initial energy hν interacts with an electron. The electron is ejected at angle ϕ with an energy $mc^2[(1-\beta^2)^{-1/2}-1]$ and a photon is emitted at angle θ with energy hν′ (Davisson & Evans, 1952).

The laws of conservation of energy and momentum can be used to write the following relationships between the angles and energies of the Compton electron and diffused photon:

$$h\nu' = \frac{h\nu}{1+\alpha(1-\cos(\theta))} \tag{52a}$$

$$E_{electron} = h\nu\left(1-\frac{1}{1+\alpha(1-\cos(\theta))}\right) \tag{52b}$$

$$\cos(\theta) = 1-\frac{2}{(1+\alpha)^2\tan^2(\phi)+1} \tag{52c}$$

$$\tan(\phi) = \frac{1}{1+\alpha}\sqrt{\frac{2}{1-\cos(\theta)}-1} \tag{52d}$$

Here, $\alpha=h\nu/mc^2$, h is the Planck's constant, υ is the incident photon frequency, m is the electron rest mass and c is the speed of light.

Klein-Nishina cross section

When a Compton interaction occurs, the energy and angle should be determined for the diffused photon and for the Compton electron. All these quantities are linked by equations (52). The probability of a photon and an electron to diffuse in directions θ and ϕ is function of the energy of the initial photon and was obtained by Klein & Nishina (1929) by solving Dirac's equation for a free electron:

$$\frac{d\sigma_{KN}(\theta)}{d\Omega} = k(\theta) = \frac{r_0^2}{2}\left\{\frac{1}{\left[1+\alpha(1-\cos(\theta)\right]^2}\left[1+\cos^2(\theta)+\frac{\alpha^2(1-\cos(\theta))^2}{1+\alpha(1-\cos(\theta))}\right]\right\} \tag{53}$$

where σ_{KN} is the Klein-Nishina cross section and $r_0=e^2/mc^2=2.82x10^{-13}$ cm[(2)]. Another important quantity is the differential cross section for Compton electrons. The laws of conservation state that probability of an electron to be deflected in the solid angle $d\Omega'$ in the direction ϕ is the same as the probability for a photon to diffuse in the solid angle $d\Omega$ in direction θ:

$$d\sigma_{KN} = k(\theta)d\Omega = k(\phi)d\Omega' \quad \text{or} \quad k(\phi) = k(\theta)(d\Omega / d\Omega') \tag{54}$$

By using relationship between angles, it can be shown that:

$$\frac{d\Omega}{d\Omega'} = -\frac{\sin(\theta)(1+\cos(\theta))}{(1+\alpha)\sin^3(\phi)} = -4\frac{(1+\alpha)^2\cos(\phi)}{\left[(1+\alpha)^2 - \alpha(2+\alpha)\cos^2(\phi)\right]^2} \tag{55}$$

Therefore $k(\phi)$, the angular distribution of Compton electron, can be calculated from Klein-Nishina differential cross section. The cross section for the Compton effect is obtained by integrating the Klein-Nishina cross section over all solid angles. This calculation gives:

$$\sigma_{KN} = 2\pi r_0^2\left[\frac{\alpha+1}{\alpha^2}\left\{\frac{2(\alpha+1)}{1+2\alpha} - \frac{1}{\alpha}\ln[1+2\alpha]\right\} - \frac{1+3\alpha}{(1+2\alpha)^2} + \frac{1}{2\alpha}\ln[1+2\alpha]\right] \tag{56}$$

Atomic form factor

The Klein-Nishina cross section was obtained by assuming that the photon interacts with an electron at rest. In reality, electrons are bound to atoms and molecules; therefore, the entire atom interacts with the incident photon. To take this into account, an *atomic form factor* S(q,Z) is introduced (Chibani, 1994):

$$\frac{d\sigma}{d\Omega} = \frac{d\sigma_{KN}}{d\Omega}S(q,Z) \tag{57}$$

where

$$q = k\sin(\theta/2) = \frac{h\nu(MeV)\sin(\theta/2)}{12.3885x10^{-3}} \tag{58}$$

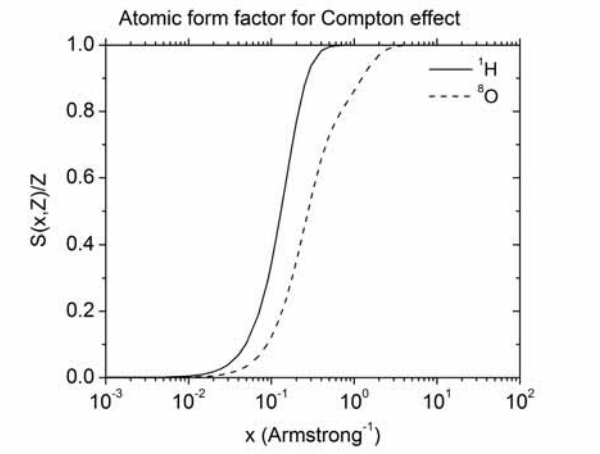
Here k is the momentum of the photon, θ is the diffusion angle of the incident photon and q is the momentum transferred to the electron ($Å^{-1}$). The function S(q,Z) increase with q, with a maximum value of Z. The effect of this form factor is to reduce the Klein-Nishina cross section. S(q,Z) also disfavor diffusion at small angles. The values of S(q,Z) were tabulated by Hubell et al. (1975) for Z from 1 to 100 and for q between 0 and 10^9 $Å^{-1}$. If a material is composed by elements Z_n in proportions p_n, S(q,Z) is replaced by:

$$S_T(q) = \sum_n p_n S(q,Z_n) \tag{59}$$

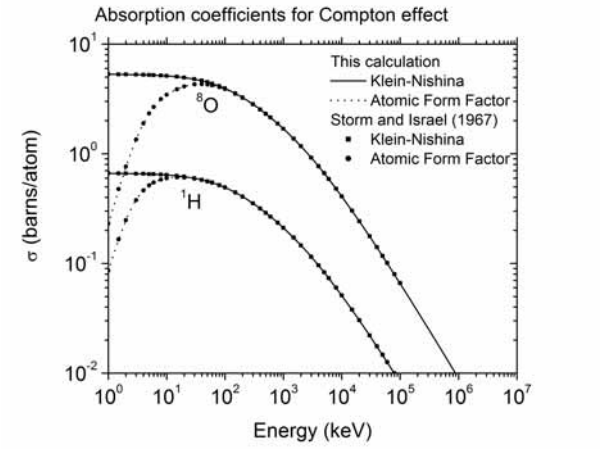
The effect of this form factor on the cross section is shown on Figure 12. It has no effect over 20 keV for ^1H and over 100 keV for ^8O.

---

[2] r_0 is also referred to as the *classical electron radius*, the radius of a spherical shell whose total electrostatic energy equals the electron rest mass



(a)



(b)

Fig. 12. (a) Atomic form factors for ^{1}H and ^{8}O for Compton effect (Hubbell et al., 1975). (b) Effect of the atomic form factor on the Compton effect cross sections for ^{1}H and ^{8}O. The data are obtained by integrating numerically the Klein-Nishina cross section multiplied by the form factor. The results are compared to the tabulated data of Storm & Israel (1967).

Sampling of the differential cross section

A method to generate angles distributed according to the Klein-Nishina cross section multiplied by the atomic form factor is needed for transport codes. If there were no atomic form factor, the algorithm of Kahn described in Raeside (1976) could be used. The following algorithm will be used instead (Plante, 2009). Let

$$x = 1 + \alpha(1 - \cos(\theta)) \tag{60}$$

The variable x varies between 1 (θ=0) and 1+2α (θ=π). The cross section may be written

$$\frac{d\sigma(\theta)}{d\Omega} = \frac{r_0^2}{x^2}\left[1 - \frac{\sin^2(\theta)}{2} + \frac{(x-1)^2}{2x}\right] \tag{61}$$

This can be sampled by rejection. The distribution $1/x^2$ (normalized) is generated from a random number U by inversion:

$$x = \frac{1+2\alpha}{1+2\alpha U} \tag{62}$$

The function between brackets is the rejection function, for which the maximum value is $(1+2\alpha)/2$. Since the rejection constant should be greater than or equal to 1, it is chosen to be 1 for $\alpha < 1/2$, or $(1+2\alpha)/2$ for $\alpha \geq 1/2$. The angle θ is calculated by using the definition of x:

$$\cos(\theta) = 1 - \frac{x-1}{\alpha} \tag{63}$$

The values of x and θ are introduced in the rejection function (RF):

$$RF = 1 - \frac{\sin^2(\theta)}{2} + \frac{(x-1)^2}{2x} \tag{64}$$

This gives algorithm 3:

Algorithm 3: Sampling of the angles for Compton effect for a photon of a given energy, given by the Klein-Nishina cross section multiplied by the form factor. The definition of x is used to calculate θ.

CALCULATE FFMax=S(E,π,Z)
IF α<1/2 { RC=1 } **ELSE** { RC=(1+2α)/2 }
REPEAT
{
Generate two random numbers R_1 and R_2 between 0 and 1

$$X = \frac{1+2\alpha}{1+2\alpha U_1}$$

$$\Theta = \cos^{-1}\left(1 - \frac{X-1}{\alpha}\right)$$

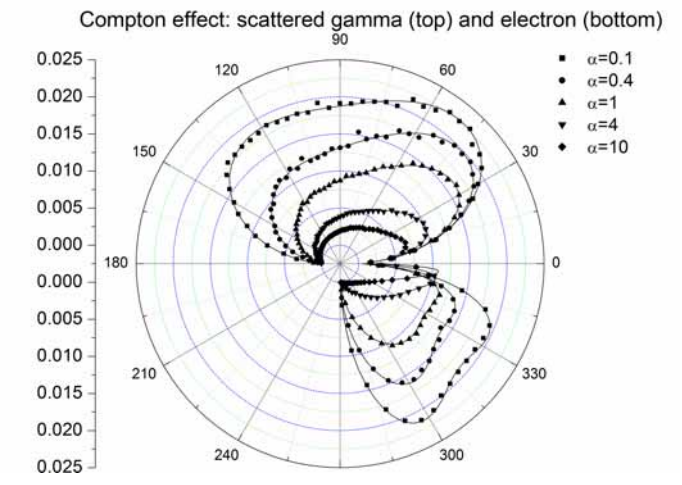
$$FR = 1 - \frac{\sin^2(\Theta)}{2} + \frac{(X-1)^2}{2X}$$

$$FF = S(E,\Theta,Z)$$

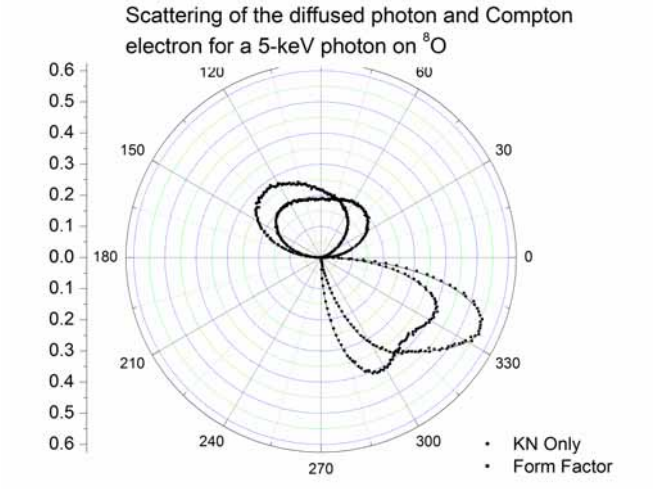
}
WHILE FFxFR < U_2xRCxFFMax
RETURN Θ ■

From the angle θ obtained with this algorithm, the energy of the scattered γ and the angle and energy of the Compton electron can be calculated. The algorithm was used 1 000 000 times to generate the distribution of angles θ and ϕ (Figure 13). The calculations were

performed for five energy values and stored in normalized histograms. There is no difference between the sampling results and the analytical curves. For the energy values used in Figure 13a, the form factor has no effect. The difference appears at low energies, such as shown on Figure 13b.



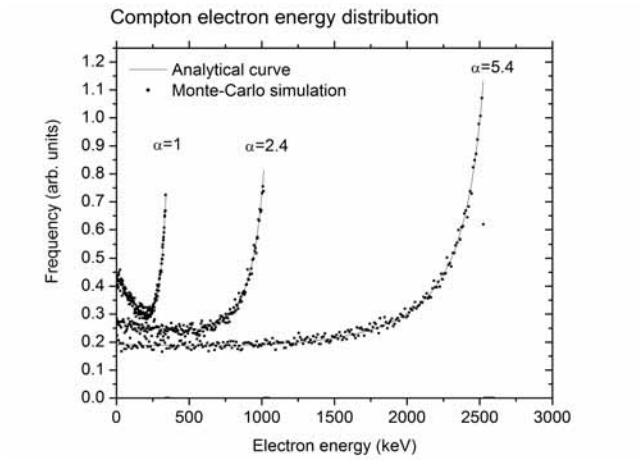
(a)



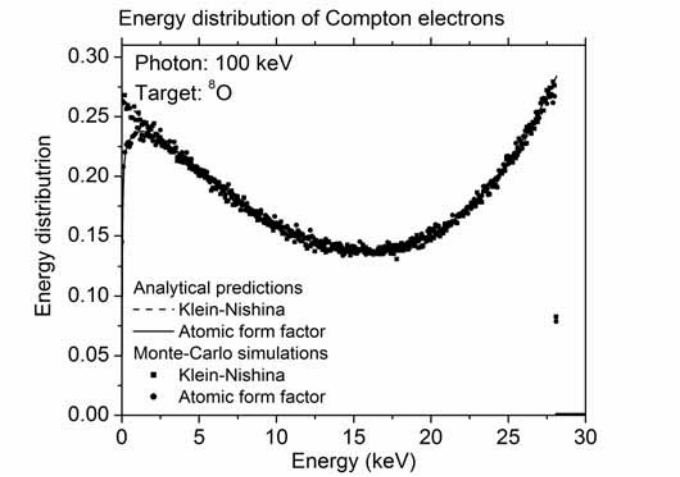
(b)

Fig. 13. a) Angular distribution of the scattered photon (top) and of the Compton electron (bottom) for initial photon energies of 0.0511 MeV, 0.2044 MeV, 0.511 MeV, 2.044 MeV and 5.11 MeV. b) Effect of the atomic form factor on the angular distributions of the scattered photon (top) and Compton electron (bottom). As usual, the lines are the analytical predictions, and the dots are given by Monte-Carlo sampling.

An important quantity that can be obtained is the energy distribution of the Compton electrons (Figure 14). The form factor is important only for low-energy photons (<100 keV).



(a)



(b)

Fig. 14. a) Distribution of Compton electron energy for photons of initial energies of 0.511 MeV, 1.226 MeV and 2.76 MeV. b) Effect of the atomic form factor on the distribution of Compton energy for photons of MeV. The lines are the analytical predictions, and the dots are obtained by Monte-Carlo simulation.

4.3.2 Coherent diffusion

When an electromagnetic wave is incident on a charged particle, the electric and magnetic components of the wave exert a Lorentz force on the particle, setting it into motion. Therefore, energy is absorbed from the incident wave by the particle and re-emitted as

electromagnetic radiation. Such a process is equivalent to the scattering of the electromagnetic wave by the particle. Its differential cross section is given by:

$$\frac{d\sigma_T}{d\Omega} = \frac{r_0^2}{2}\left[1+\cos^2(\theta)\right] \tag{65}$$

The total cross section σ_T[3] is calculated by integrating $d\sigma_T/d\Omega$ over all solid angles:

$$\sigma_T = \int \frac{d\sigma_T}{d\Omega} d\Omega = 2\pi \int_0^{\pi} \frac{r_0^2}{2}[1+\cos^2(\theta)]\sin(\theta)d\theta = \frac{8\pi r_0^2}{3} \tag{66}$$

Atomic form factor

According to equation (66), the coherent diffusion cross section is not function of the photon energy, which is obviously not the case (see absorption coefficients). As for Compton effect, an atomic form factor should be introduced (Chibani, 1994):

$$\frac{d\sigma_T}{d\Omega} = \frac{r_0^2}{2}[1+\cos^2(\theta)]\left|F(q,Z_n)\right|^2 \tag{67}$$

The values of F(q,Z) were tabulated by Hubell & Øverbø (1979). If a material is composed of elements Z_n in proportions p_n, $|F(q,z)|^2$ is replaced by:

$$F_T(q) = \sum_n p_n \left|F(q,z_n)\right|^2 \tag{68}$$

The effect of the atomic form factor on the cross sections is shown on Figure 15.

Sampling of the coherent diffusion cross section

An algorithm to generate angles corresponding to the coherent diffusion cross section is needed. The differential cross may be written

$$\frac{d\sigma_T}{d\theta} = r_0^2[1+\cos^2(\theta)]\left|F(q,Z_n)\right|^2 \frac{\sin(\theta)}{2} \tag{69}$$

The distribution $\sin(\theta)/2$ is normalized; therefore, a random number Θ with such distribution can be generated by the inversion method (R is an uniform random number between 0 and 1):

$$\Theta = \cos^{-1}(1-2R) \tag{70}$$

The rejection function is therefore

$$RF = \left(\frac{F(q,Z)}{Z}\right)^2 \left(\frac{1+\cos^2(\theta)}{2}\right) \tag{71}$$

This gives the algorithm to generate angles distributed as coherent diffusion.

[3] σ_T is the Thompson cross section

Algorithm 4: Algorithm to sample the coherent diffusion angles. The maximal value of F(q,Z) is Z.

REPEAT

{

Generate two random numbers R_1 and R_2 between 0 and 1

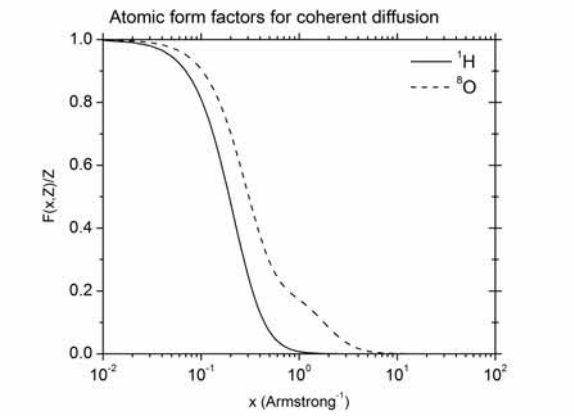
$$\Theta = \cos^{-1}(1 - 2R_1)$$

$$FR = \left(\frac{F(q,Z)}{Z}\right)^2 \left(\frac{1+\cos(\Theta)}{2}\right)$$

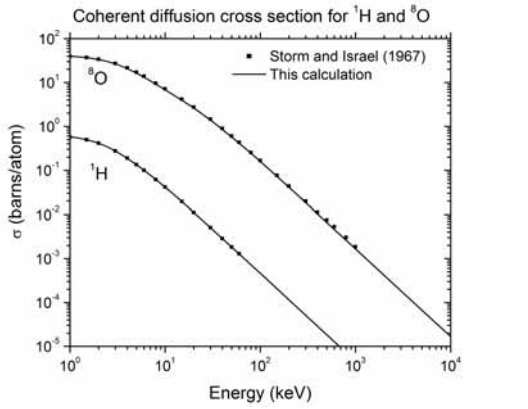
}

WHILE $FR*R_2 > R_1$

RETURN Θ ■



(a)



(b)

Fig. 15. a) Atomic form factors for coherent diffusion on ^{1}H and ^{8}O. (Hubbell et al., 1975). b) Coherent diffusion cross section for ^{1}H and ^{8}O calculated by integrating numerically the differential cross section multiplied by the atomic form factor. The results are compared with tabulated data of Storm & Israel (1967).

Simulation results (dots) are compared with the analytical curves of Figure 13. The dots are so close to the analytical functions that the lines are not seen.

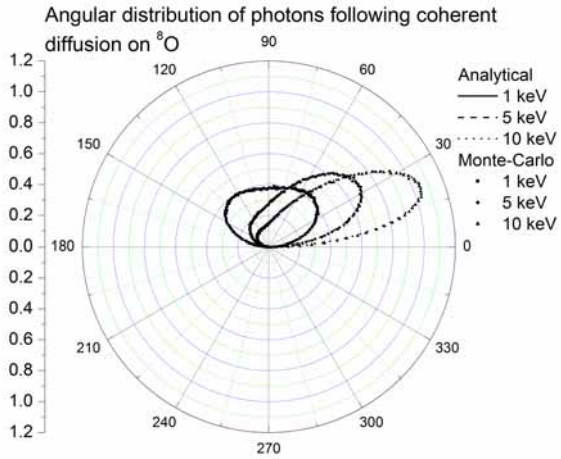


Fig. 16. Sampling of the angular distribution for photon of 1 keV, 5 keV and 10 keV on ^{8}O, taking the atomic form factor into consideration. The dots are obtained by Monte-Carlo simulation by sampling the algorithm 1000000 times. The lines are the analytical predictions.

4.3.3 Photoelectric effect

Photoelectric effect is the process by which an orbital electron absorbs the energy of an incident photon and is ejected. The energy of the electron is the photon energy minus the binding energy of the electron. The photons that have an energy greater than the binding energy of the K shell of Oxygen, I_K=539.7 eV, interacts only with those electrons. Otherwise, the binding energy I_L =19.6 eV is assumed.

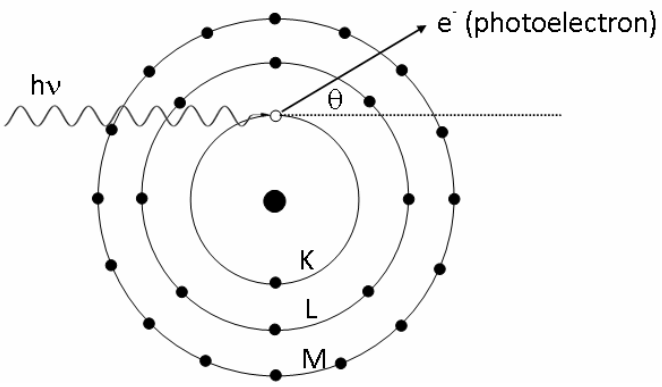


Fig. 17. Photoelectric effect. The probability of interaction is higher with internal electrons, which are more strongly bound.

Since a free electron cannot absorb a photon (this is not allowed by the laws of conservation of momentum and energy), photoelectric effect can only occur on a bound electron. In fact, the probability of photoelectric effect increases with the binding energy of the electron (Heitler, 1954). In (Anderson, 1984; Storm & Israel, 1967), an empirical formula gives the ratio of the total photoelectric cross section (σ_τ) to K layer photoelectric cross section (σ_K):

$$\sigma_\tau / \sigma_K = 1 + 0.01481(\ln(Z))^2 - 0.00079(\ln(Z))^3 \tag{72}$$

For oxygen, if $\sigma_\tau=\sigma_K+\sigma_L$, the calculation gives $\sigma_L=0.057\sigma_K$. Some authors (Hill & Smith, 1996; Turner et al., 1980) assumed that photons which energy is higher than the binding energy of the K shell of oxygen, I_K=539.7 eV, interact only with these electrons. For lower energy, the binding energy I_L =19.6 eV is assumed. When an electron of the K shell is emitted, an Auger electron of energy E_{Auger}=520.1 eV is also emitted (Hill & Smith, 1996). Note that Turner et al. (1980), which has performed similar calculations, have used I_K=532 eV, I_L=12 eV and E_{Auger} = 508 eV.

The cross section for the photoelectric effect is harder to calculate analytically than in the case of Compton effect, because Dirac's equation should be solved for bound electrons. In this work, Sauter's formula for the angular distribution of photoelectrons is used (Sauter, 1931). It can be written (Tseng et al, 1978):

$$\frac{d\sigma_\tau}{d\Omega} = \frac{\lambda \sin^2(\theta)}{[1-\beta\cos(\theta)]^4}\{1+\kappa[1-\beta\cos(\theta)]\} \tag{73}$$

Where

$$\kappa = \gamma\left(-\frac{1-\sqrt{1-\beta^2}}{2\sqrt{1-\beta^2}} + \frac{\left(1-\sqrt{1-\beta^2}\right)^2}{2(1-\beta^2)}\right) = \frac{\gamma(\gamma-1)(\gamma-2)}{2} \tag{74}$$

$$\lambda = \frac{4Z^5\alpha\beta(\gamma+1)}{(\gamma-1)^4\gamma^3} = \frac{4Z^5\alpha\beta(\gamma+1)n^4}{\gamma^3} \tag{75}$$

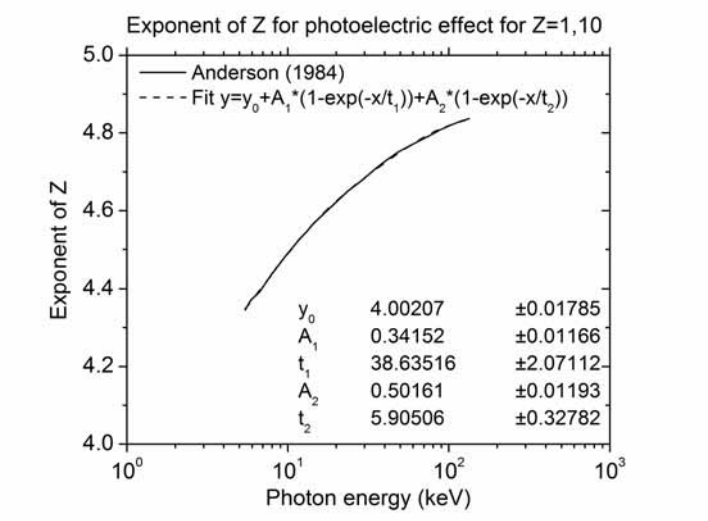
Here, $\alpha = e^2/\hbar c$ is the structure fine constant, EB is the binding energy of the electron, n is the energy in units of electron rest mass ($n=h\upsilon/mc^2$) and

$$\gamma = \frac{1}{\sqrt{1-\beta^2}} = \frac{h\nu - E_B + mc^2}{mc^2} 1 + 1/n \tag{76}$$

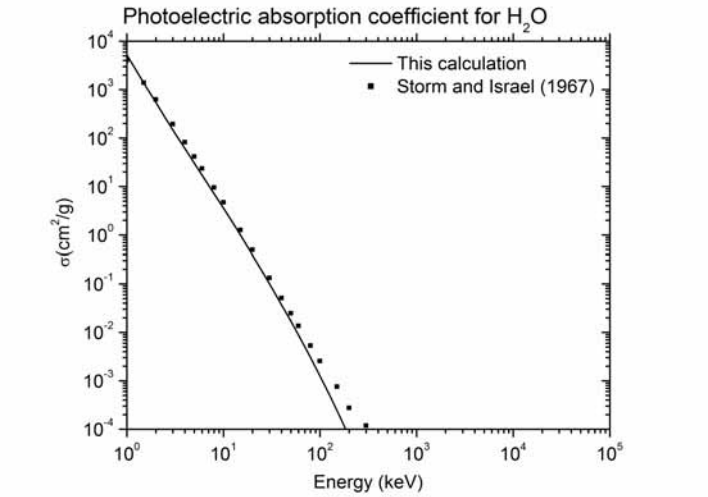
The total cross section is calculated by integrating $d\sigma_\tau/d\Omega$ over all solid angles. This yields the results given in Davisson & Evans (1952):

$$\sigma_\tau = \frac{3}{2}\varphi_0 \frac{Z^5}{(137)^4} n^5(\gamma^2-1)^{3/2}\left[\frac{4}{3} + \frac{\gamma(\gamma-2)}{\gamma+1}\left[1 - \frac{1}{2\gamma\sqrt{\gamma^2-1}}\ln\left(\frac{\gamma+\sqrt{\gamma^2-1}}{\gamma-\sqrt{\gamma^2-1}}\right)\right]\right] \tag{77}$$

The photoelectric cross section cannot reproduce properly the absorption cross section of photoelectric effect for water. This difference comes from the fact that Z varies with energy (Anderson, 1984). However, using a variable exponent in the calculation of σ_τ, the cross section is very similar to the data of Storm & Israel (1967). This is illustrated on Figure 18.



(a)



(b)

Fig. 18. a) Exponent Z as a function of the photon energy for photoelectric effect.
b) Photoelectric absorption coefficients calculated from Sauter's formula, including the variation of the exponent as function of the energy.

To find the angular distribution of photoelectrons, Sauter's distribution is written as:

$$d\sigma_\tau = \frac{2\pi\lambda\sin^3(\theta)}{[1-\beta\cos(\theta)]^4}\{1+\kappa[1-\beta\cos(\theta)]\}d\theta \tag{78}$$

Introducing $u = \cos(\theta)$, the distribution takes a simpler form:

$$f(u) \propto \frac{1-u^2}{(1-\beta u)^4}\left[1+\kappa(1-\beta u)\right] \tag{79}$$

This function can be sampled by rejection. We define g(u) and h(u), such as $f(u) \propto g(u)h(u)$, g(u) is normalized and $h(u) \geq 1$:

$$g(u) = \frac{1}{2\gamma^2(\kappa+\gamma^2)}\frac{\left[1+\kappa(1-\beta u)\right]}{(1-\beta u)^3} \tag{80}$$

$$h(u) = \frac{\gamma-1}{2\gamma}\left(\frac{1-u^2}{1-\beta u}\right) \tag{81}$$

The function g(u) can be sampled by inversion, by solving the following equation for Y:

$$R = \int_{-1}^{Y} \frac{1}{2\gamma^2(\kappa+\gamma^2)}\frac{\left[1+\kappa(1-\beta u)\right]}{(1-\beta u)^3}du \tag{82}$$

The integral yields[4]:

$$R = \frac{1}{4\beta\gamma^2(\kappa+\gamma^2)}\left[\frac{1}{(1-\beta Y)^2}+\frac{2\kappa}{(1-\beta Y)}-\frac{1}{(1+\beta)^2}-\frac{2\kappa}{(1+\beta)}\right] \tag{83}$$

By completing squares, we find:

$$R = \frac{1}{4\beta\gamma^2(\kappa+\gamma^2)}\left[\left(\kappa+\frac{1}{1-\beta Y}\right)^2-\left(\kappa+\frac{1}{1+\beta}\right)^2\right] \tag{84}$$

It is now possible to isolate Y (Kawrakow & Rogers, 2003):

$$Y = \frac{1}{\beta}\left[1-\left(\sqrt{4\beta\gamma^2(\kappa+\gamma^2)R+\left(\kappa+\frac{1}{1+\beta}\right)^2}-\kappa\right)^{-1}\right] \tag{85}$$

This gives the algorithm 5, which may be used to sample the photoelectrons angular distribution.

---

[4] The normalization of g(u) is verified by using Y=1 in the equation, i.e. $\int_{-1}^{1} g(u)du = 1$

Algorithm 5: Sampling of the Sauter's angular distribution of photoelectrons. The quantities β, γ and κ are defined in the text.
CALCULATE β, γ and κ
REPEAT
{

Generate two random numbers R_1 and R_2 uniformly disbributed between 0 and 1

$$Y = \frac{1}{\beta}\left[1 - \left(\sqrt{4\beta\gamma^2(\kappa+\gamma^2)R_1 + \left(\kappa + \frac{1}{1+\beta}\right)^2} - \kappa\right)^{-1}\right]$$

$$h(Y) = \frac{\gamma - 1}{2\gamma}\left(\frac{1 - Y^2}{1 - \beta Y}\right)$$

}
WHILE $R_2 > h(Y)$
RETURN $\Theta = \cos^{-1}(Y)$ ■

The angular distribution obtained by using the preceding algorithm is compared to Sauter's distribution on Figure 19.

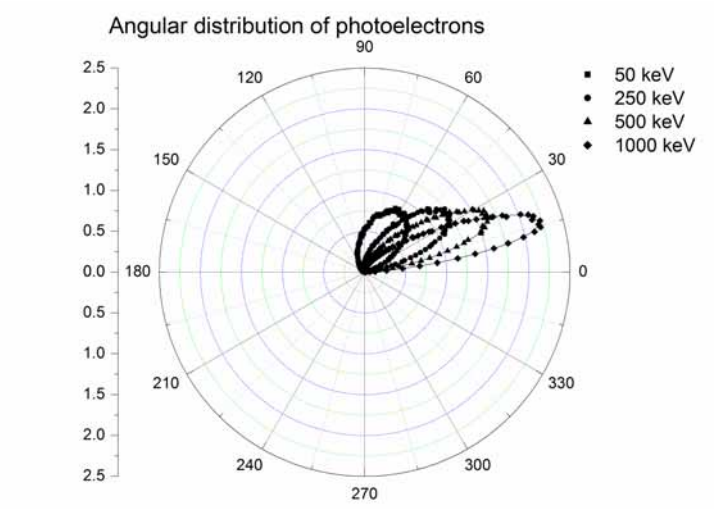


Fig. 19. Angular distribution of photoelectrons obtained by sampling Sauter's formula 100000 times with the algorithm. The dots are obtained by Monte-Carlo simulation. The lines are the analytical predictions (Sauter's distribution).

5. Simulation results

In this section, simulation results obtained with the Monte-Carlo transport code RITRACKS are shown.

5.1 Electrons

5.1.1 Electron range

The range of electrons of energies up to 150 keV in liquid water has been calculated by Meesungnoen et al. (2002) and up to 100 keV by Uehara & Nikjoo (2006). Figure 20 displays the computed values of the electron penetration as a function of initial electron energy from 0.1 eV to 10 MeV calculated with RITRACKS by using the relativistic and the non-relativistic cross sections. Experimental results from Konovalov et al. (1988) are also shown.

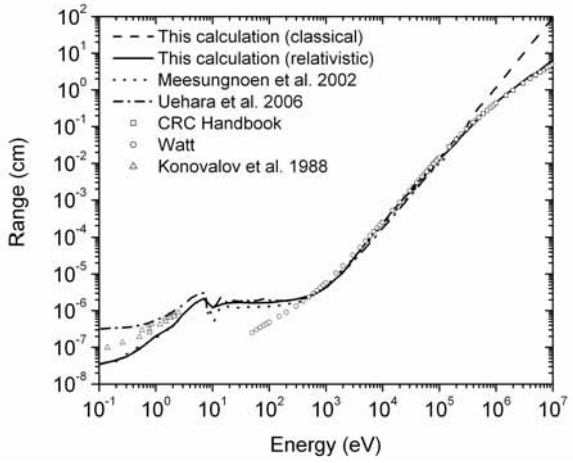


Fig. 20. Electron range in liquid water. The calculations have been performed using the classical and relativistic cross sections. Data from Meesungnoen et al. (2002), Uehara and Nikjoo (2006), Watt (1996), the CRC Handbook (Brodsky, 1978) and Konovalov et al. (1988) are also shown.

The results obtained below 150 keV are similar to those from Meesungnoen et al. (2002); the reader is thus referred to this article for a more detailed discussion of this curve below 150 keV. Only major points will be recalled here. In the subexcitation electron energy range (<7.3 eV), the penetration range is often called the "thermalization distance". It increases from ~0.35 nm at 0.1 eV to ~18 nm at 7.3 eV. This problem has been extensively studied (Goulet et al. 1990); the results of RITRACKS are in good agreement with the reported values. Three minimas in the electron range curve are reported by Meesungnoen et al. (2002) at ~11, 22 and 30-35 eV; however, they are not clearly seen in figure 11 because the energy steps used between each point is too large. Between 30 and 300 eV, the calculated range increases very slowly, also in agreement with the calculation from Meesungnoen et al. (2002). To our knowledge, there are no experimental data between ~5-50 eV, where the minimas are predicted by Meesungnoen et al. (2002) and by Uehara and Nikjoo (2006). Between 300 eV and 150 keV, there is an excellent agreement of our calculations with the values from the CRC Handbook (Brodsky, 1978) and the book of Watt (1996). Over ~150 keV, the difference in the electron range calculated with the relativistic and the non-relativistic cross sections appears. This is discussed in Plante & Cucinotta (2009). At high energy, the relativistic cross sections needs to be used to have the calculation of the electron range in agreement with data from Watt (1996) and the CRC Handbook (Brodsky, 1978)

5.1.2 Stopping power

The stopping power[5] is another very important quantity that was used to validate the RITRACKS code. The calculation has been performed by Gümüş (2005) and Paretzke (see Dingfelder et al., 2008). Stopping power data are found in the CRC handbook (Brodsky, 1978); Watt, 1996; ICRU 37 (1984), ICRU 16 (1970) and IAEA (1995). The available data for stopping power exists with and without the bremsstrahlung. The stopping power was calculated by RITRACKS (figure 21) with Rudd's formulae for energies <150 keV. At higher energies, relativistic corrections to cross sections and bremsstrahlung needs to be added, but this will not be discussed here (see Plante & Cucinotta, 2009). There is excellent agreement of the results with the existing data in all range, but the agreement is the best between ~1 keV and ~100 keV.

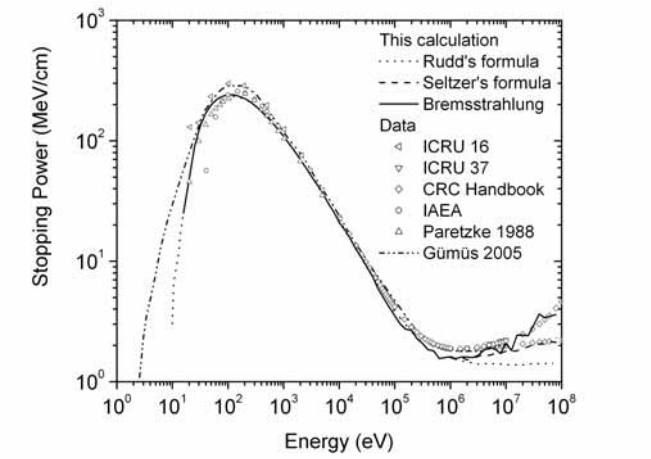


Fig. 21. Electron stopping power, calculated without bremsstrahlung using Rudd's relativistic formula and Seltzer's formulae. Data without bremsstrahlung from CRC Handbook (Brodsky, 1978), Gümüş (2005), Paretzke (Dingfelder et al., 2008), ICRU 16 (1970) and ICRU 37 (1984) and with bremsstrahlung from CRC Handbook (Brodsky, 1978) are also shown.

5.2 Ions

5.2.1 Tracks

On Figure 22, XY plane projections of track segments calculated at ~10^{-12} s are shown for $^{4}He^{2+}$, $^{12}C^{6+}$, $^{28}Si^{14+}$ and $^{56}Fe^{26+}$ ions (LET ~150 keV/μm). Even if the ions have the same LET, their structure are very different. The central region of the track is the so-called *core* of the track, and results from the dense ionization created by the ion. The peripherical region, the *penumbra*, is created by the trajectories of the secondary electrons ionized by the primary ion. As discussed previously, the maximum energy that can be transferred to an electron is proportional to the energy per nucleon of the ion. This is exactly what is observed here: the higher the energy per nucleon, the more energetic are the secondary electrons and the larger the penumbra.

[5] The stopping power is closely related to the linear energy transfer (LET), except that the LET does not include radiative loss (such as bremsstrahlung).

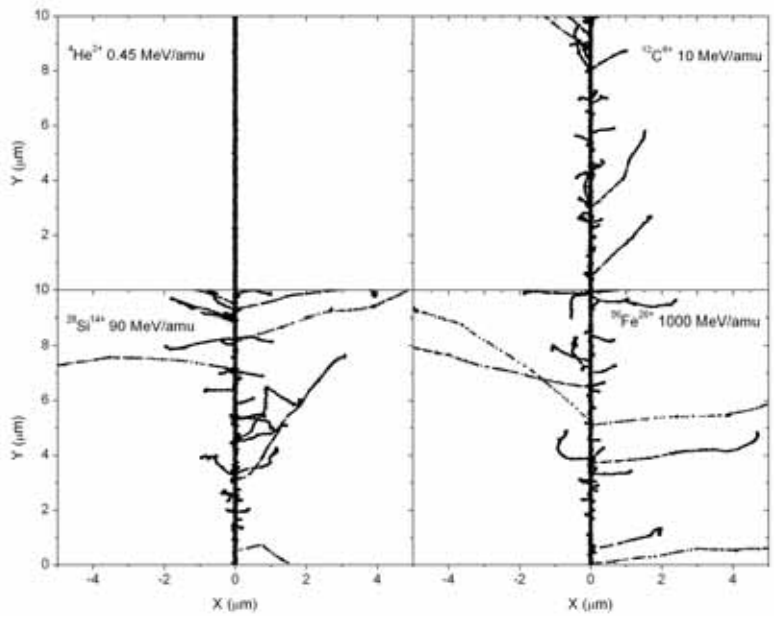


Fig. 22. Projections over the XY plane of simulated tracks segments (calculated at ~10^{-12} s) for the following impact ions: $^{4}He^{2+}$ (0.45 MeV/amu), $^{12}C^{6+}$ (10 MeV/amu), $^{28}Si^{14+}$ (90 MeV/amu) and $^{56}Fe^{26+}$ (1 GeV/amu). Ions are generated at the origin along the Y axis in liquid water at 25 °C under identical LET conditions (~150 keV/μm). Each dot represents a radiolytic species.

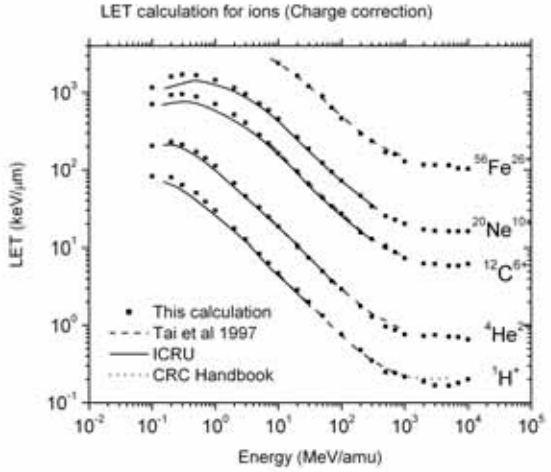


Fig. 23. Calculation of the LET as a function of the energy for $^{1}H^{+}$, $^{4}He^{2+}$, $^{12}C^{6+}$, $^{20}Ne^{10+}$ and $^{56}Fe^{26+}$ using the cross sections shown above and including charge effects and relativistic corrections.

5.2.2 Stopping power

The stopping power (or LET) was calculated as function of the energy for the ions $^{1}H^{+}$, $^{4}He^{2+}$, $^{12}C^{6+}$, $^{20}Ne^{10+}$ and $^{56}Fe^{26+}$ (Figure 23). In general, results are in good agreement with the calculations derived from other codes (Tai et al., 1997), ICRU values (ICRU 1993) and CRC Handbook values (Brodsky, 1978), for all ions and the energy range considered (~10^{-1}-10^{4} MeV/amu).

5.2.3 Radial dose

The radial dose is of interest for microdosimetric applications and was also used to validate the results of the RITRACKS code. It is calculated by recording the energy deposited and the radial distance from the Y axis of the energy loss events. The energy deposited in each differential volume element is then divided by its volume and converted to Gy. The calculated radial dose for a 1-MeV $^{1}H^{+}$ ion (Figure 24) are in good agreement with previous amorphous tracks calculations (Cucinotta et al. 1998). Radial dose profiles for other ions are shown in (Plante & Cucinotta, 2008).

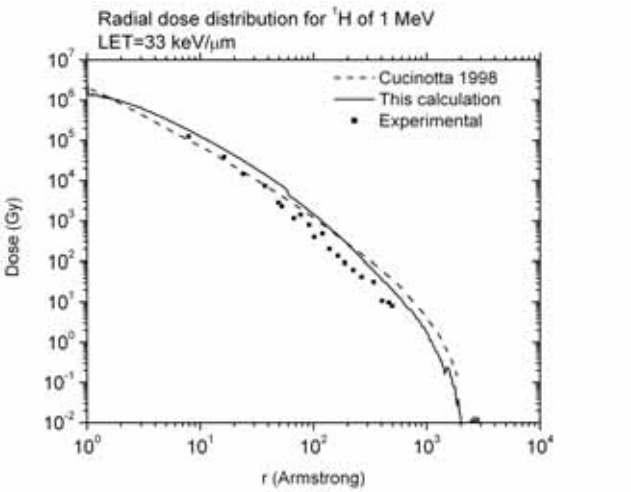


Fig. 24. Calculation of radial dose profiles for $^{1}H^{+}$, 1 MeV (LET~33 keV/μm). Amorphous track calculations and experimental data from Cucinotta et al. (1998) are also shown.

5.3 Photons

5.3.1 Number of electrons emitted per photon

Simulations have been performed with photons of energies up to 2 MeV. Figure 25 shows the number of electrons generated per incident photon. This calculation is compared with previous results from Turner (1980). The curve seems to plateau at about 17 electrons per photon. This is explained by the fact that the Compton electrons spectra is more intense near the maximal energy transfer, with is a more important fraction of the initial energy when the initial photon energy is large. Thus, a photon will lose an important fraction of its energy during the first collisions. At low energies, we note that at least two electrons are emitted. This is due to the emission of the Auger electron.

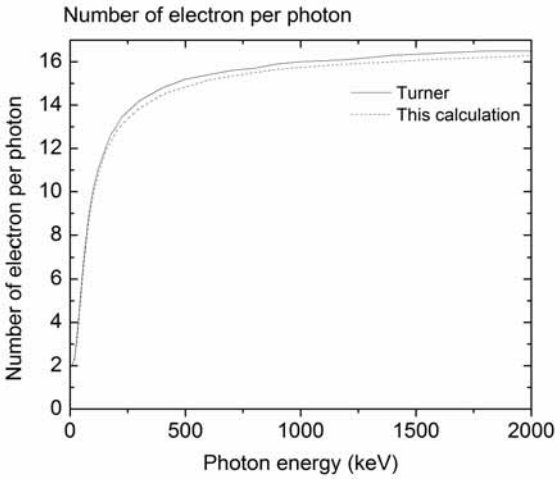


Fig. 25. Number of electrons emitted per photon, as function of the initial photon energy.

5.3.2 Energy distribution of the secondary electrons

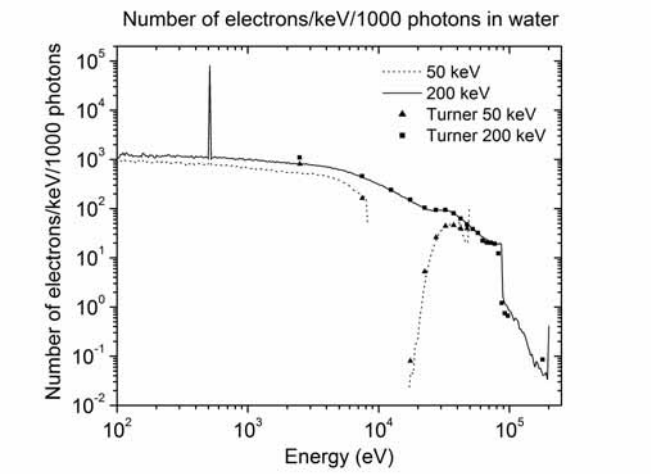
A very important quantity that is calculated by the program is the distribution of the energy of the secondary electrons, resulting from the slowing down of photons. The calculation has been performed for 50 keV, 200 keV, 1 MeV, 1.2 MeV, 1.4 MeV, 1.6 MeV, 1.8 MeV and 2.0 MeV. Our results are shown on Figure 26 and compared with results from Turner et al. (1980). Although a very different approach has been used by Turner to sample the cross sections, the results are similar in all cases. The peak that is seen at 500 eV corresponds to Auger electrons.

6. Conclusion

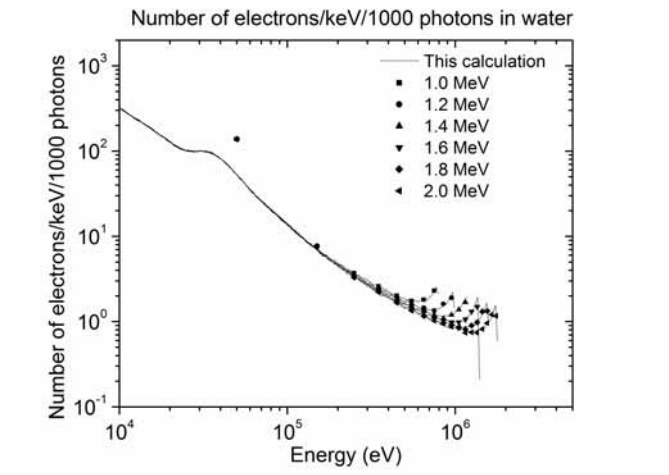
Ionizing radiations comprises several types of energetic particles such as electrons, protons, α-particles and photons (X-rays or γ-rays). They are produced by natural processes and by man-made devices and are widely used in medical applications for diagnostic procedures and cancer treatment. In space, HZE particles are also present and may be a concern for long-term manned missions.

Several health risks are associated with radiation exposure. The increase in cancer risk is the most studied; however, ionizing radiation may also increase the risk of degenerative diseases of the cardio-vascular and central nervous systems. The biological pathways involved in the effects of radiations are complex, but they are initiated by physical, physico-chemical and chemical interactions with the medium. Therefore much effort has been invested over last decades to understand these processes.

Because of the stochastic nature of radiation interactions, Monte-Carlo simulations are very useful to study ionizing radiations. They have greatly helped our understanding of the physical interactions of radiation with matter. Over the years, they have also become more accessible thanks to the availability of computer power and storage capacity. As new cross sections data become available, the models of radiation interaction are continuously improving over time. Therefore, Monte-Carlo simulations are now indispensable tools that are used in many applications such as in radiotherapy treatment planning and in fundamental research.



(a)



(b)

Fig. 26. Distribution of the energy of the secondary electrons created by irradiation of liquid water with photons. This calculation (lines) and results from Turner (1980).

7. Acknowledgements

We would like to thank Prof. Jean-Paul Jay-Gerin (University of Sherbrooke) for helpful discussions.

8. References

Anderson, D.W. (1984). *Absorption of Ionizing Radiation*, University Park Press, ISBN: 083911821X, Baltimore, Md.

Barkas, H. (1963). *Nuclear Research Emulsions Vol. 1*, Chapter 9, p. 371, Academic Press, ISBN: 0120783010, New York, NY

Boudaïffa, B.; Cloutier, P.; Hunting, D.; Huels, M.A. & Sanche, L. (2000). Resonant formation of DNA strand breaks by low energy (3 to 20 eV) electrons. *Science*, 287, 1658-1659. ISSN: 0036-8075

Brenner, D.J. & Zaider, M. (1983). A computationally convenient parameterisation of experimental angular distributions of low energy electrons elastically scattered off water vapour. *Phys. Med. Biol.*, 29 443-447. ISSN: 0031-9155.

Brodsky, A.B. (1978). *CRC Handbook of Radiation Measurement and Protection*. CRC Press, ISBN: 9780849337703, West Palm Beach, Fl.

Chibani, O. (1994). *Simulation du transport de particules (Photons, électrons et positrons) – Le système GEPTS*. Ph.D. thesis, Université Paul Sabatier, Toulouse, France.

Cobut, V. (1993). *Simulation Monte Carlo du transport d'électrons non relativistes dans l'eau liquide pure et de l'évolution du milieu irradié: rendements des espèces créées de 10^{-15} à 10^{-7} s.* Ph.D. thesis, Université de Sherbrooke, Québec, Canada.

Cobut V.; Frongillo, Y.; Patau, J.P.; Goulet, T.; Fraser, M.-J. & Jay-Gerin, J.-P. (1998). Monte-Carlo simulation of fast electron and proton tracks in liquid water - I. Physical and physicochemical aspects. *Radiat. Phys. Chem.*, 51, 229-243. ISSN: 0969-806X

Cucinotta, F.A. & Durante, M. (2006). Cancer risk from exposure to galactic cosmic rays: implications for space exploration by human beings. *Lancet Oncol.*, 7, 431-435. ISSN: 1470-2045

Cucinotta, F.A.; Katz, R. & Wilson, J.W. (1998). Radial distribution of electron spectra from high-energy ions. *Radiat. Env. Biophys.*, 37, 259-265. ISSN : 0301-634X

Danjo, A. & Nishimura, H. (1985). Elastic scattering of electrons from the H_2O molecule. *J. Phys. Soc. Jpn.*, 54, 1224-1227. ISSN: 0031-9015

Davisson, C.M. & Evans, R.D. (1952). Gamma rays absorption coefficients. *Rev. Mod. Phys.*, 24, 79-107. ISSN: 0034-6861

Devroye, L. (1986). *Non-Uniform Random Variate Generation*. Springler-Verlag, New York. ISBN: 978-0387963051

Dingfelder, M.; Jorjishvili, I.G.; Gersh, J.A. & Toburen, L.H. (2006). Heavy ion track structure simulation in liquid water at relativistic energies. *Radiat. Prot. Dosim.*, 122, 26-27. ISSN: 0144-8420

Dingfelder, M.; Ritchie, R.H.; Turner, J.E.; Friedland, W.; Paretzke, H.G. & Hamm, R.N. (2008). Comparisons of calculations with PARTRAC and NOREC: transport of electrons in liquid water. *Radiat. Res.*, 169, 584-594. ISSN: 1938-5404

Goulet, T.; Patau, J.-P. & Jay-Gerin, J.-P. (1990). Thermalization and recombination of subexcitation electrons in solid water. *Radiat. Prot. Dosim.*, 31, 33-36. ISSN: 0144-8420

Gümüş, H. (2005) Simple stopping power formula for low and intermediate energy electrons. *Radiat. Phys. Chem.*, 72, 7-12. ISSN: 0969-806X

Hill, M.A. & Smith, F.A. (1996). Is the response of the Fricke dosimeter constant for high energy electrons and photons? *Radiat. Phys. Chem.*, 47, 637-647. ISSN: 0969-806X

Hubbell, J.H.; Veigele, W.J.; Briggs, E.A.; Brown, R.T.; Cromer, D.T. & Howerton, R.J. (1975). Atomic form factors, incoherent scattering functions and photon scattering cross sections. *J. Phys. Chem. Ref. Data*, 4, 471-538. ISSN: 0047-2689

Hubbell, J.H. & Øverbø, I. (1979). Relativistic atomic form factors and photon coherent scattering cross sections. *J. Phys. Chem. Ref. Data*, 8, 69-106. ISSN: 0047-2689

ICRU (1984). *Stopping Powers and Ranges for Electrons and Positrons*. ICRU Report 37. International Commission on Radiation Units and Measurements, Bethesda, Md.

ICRU (1970). *Linear Energy Transfer*. ICRU Report 16. International Commission on Radiation Units and Measurements, Bethesda, Md.

ICRU (1993). *Stopping Powers and Ranges for Protons and Alpha Particles*. ICRU Report 49. International Commission on Radiation Units and Measurements, Bethesda, Md.

IAEA (1995). *Atomic and Molecular Data for Radiotherapy and Radiation Research*. IAEA-TECDOC-799, IAEA, Vienna

Jay-Gerin, J.-P. & Ferradini, C. (1999). La radiolyse de l'eau et des solutions aqueuses: historique et actualité. *Can. J. Chem.* 77, 1542-1575. ISSN: 0008-4042

Kawrakow, I. & Rogers, D.W.O. (2003). *The EGSnrc Code System: Monte Carlo Simulation of Electron and Photon Transport*. NRCC Report PIRS-701.

Katase, A.; Ishibashi, K.; Matsumoto, Y.; Sakae, T.; Maezono, S.; Murakami, E.; Watanabe, K. & Maki, H. (1986). Elastic scattering of electrons by water molecules over the range 100-1000 eV. *J. Phys. B*, 19, 2715-2734. ISSN: 0022-3700

Klein, O. & Nishina, Y. (1929). Über die Streuung von Strahlung durch freie Elektronen nach der neuen relativistischen Quantendynamik von Dirac. *Z. Phys.*, 52, 853-868. ISSN: 0044-3328

Konovalov, V.V.; Raitsimring, A.M. & Tsvetkov, Yu.D. (1988). Thermalization lengths of "subexcitation electrons" in water determined by photoinjections from metals into electrolyte solutions. *Radiat. Phys. Chem.*, 32, 623-632. ISSN: 0969-806X

Kutcher, G.J. & Green, A.E.S. (1976). A model for energy deposition in liquid water. *Radiat. Res.*, 67, 408-425. ISSN: 1938-5404

Meesungnoen, J.; Jay-Gerin, J.-P.; Filali-Mouhim, A. & Mankhetkorn, S. (2002). Low-energy electron penetration range in liquid water. *Radiat. Res.*, 158, 657-660. ISSN: 1938-5404

Michaud, M.; Wen, A. & Sanche, L. (2003). Cross sections for low-energy (1-100 eV) electron elastic and inelastic scattering in amorphous ice. *Radiat. Res.*, 159, 3-22. ISSN: 1938-5404

Mozumder, A. & Magee, J.L. (1966). Theory of radiation chemistry, VII. Structure and reaction in low LET tracks. *J. Chem. Phys.*, 45, 3332–3341. ISSN: 0021-9606

Nikjoo, H.; Uehara, S., Emfietzoglou, D. & Cucinotta, F.A. (2006). Track-structure codes in radiation research. *Radiat. Meas.*, 41, 1052–1074. ISSN: 1350-4487

Nikjoo, H.; Uehara, S.; Emfietzoglou, D. & Brahme, A. (2008). Heavy charged particles in radiation biology and biophysics. *New J. Phys.*, 10, 1-28. ISSN: 1367-2630

O'Neill, P. & Wardman, P. (2009). Radiation chemistry comes before radiation biology. *Int. J. Radiat. Biol.*, 85, 9-25. ISSN: 0955-3002

Pimblott, S.M. & LaVerne, J.A. (2007). Production of low-energy electrons by ionizing radiation. *Radiat. Phys. Chem.*, 76, 1244-1247. ISSN: 0969-806X

Plante, I. & Cucinotta, F.A. (2008). Ionization and excitation cross sections for the interaction of HZE particles in liquid water and application to Monte-Carlo simulation of radiation tracks. *New J. Phys.* 10, 125020. ISSN: 1367-2630

Plante, I. & Cucinotta, F.A. (2009). Cross sections for the interactions of 1 eV – 100 MeV electrons in liquid water and application to Monte-Carlo simulation of HZE radiation tracks. *New J. Phys.*, 11, 063047. ISSN: 1367-2630

Plante, I. (2009). Développement de codes de simulation Monte-Carlo de la radiolyse de l'eau par des électrons, ions lourds, photons et neutrons. Applications à divers sujets d'intérêt expérimental. Ph.D. thesis, Université de Sherbrooke, Québec, Canada.

Powell, C.J.; Jablonski, A. & Salvat, F. (2005). NIST databases with electron elastic-scattering cross sections, inelastic mean free paths, and effective attenuation lengths *Surf. Interface Anal.*, 37, 1068-1071. ISSN: 0142-1421

Press, W.H.; Teukolsky, S.A.; Vetterling, W.T. & Flannery, B.P. (1992). *Numerical Recipes in Fortran*. 2nd Edition, Cambridge University Press, ISBN: 978-0521880688, Cambridge.

Raeside, D.E. (1976). Monte-Carlo principles and applications. *Phys. Med. Biol.*, 21, 181-197. ISSN: 0031-9155.

Reynaert, N.; van der Marck, S.C.; Schaart, D.R.; Van der Zee, W.; Van Vliet-Vroegindeweij, C.; Tomsej, M.; Jansen, J.; Heijmen, B.; Coghe, M. & De Wagter, C. (2007). Monte Carlo treatment planning for photon and electron beams. *Radiat. Phys. Chem.*, 76, 643-686. ISSN: 0969-806X

Rowntree, P.; Parenteau, L. & Sanche, L. (1991). Electron stimulated desorption via dissociative attachment in amorphous H_2O. *J. Chem. Phys.*, 94, 8570-8576. ISSN: 0021-9606

Rudd, M.E. (1990). Cross sections for production of secondary electrons by charged particles. *Radiat. Prot. Dosim.*, 31, 17-22. ISSN: 0144-8420

Sauter, F. (1931). Über den Atomaren Photoeffekt in der K-Schale nach der Relativistischen Wellenmechanik Diracs. *Ann. Phys.*, 11, 454-488. ISSN: 0003-4916

Storm, E. & Israel, H.I. (1967). *Photon Cross Sections from 0.001 to MeV for Elements 1 through 100*. Los Alamos Scientific Laboratory report 3753, New Mexico.

Tai, H.; Bichsel, H.; Wilson, J.W.; Shinn, J.L.; Cucinotta, F.A. & Badavi, F.F. (1997). Comparison of stopping power and range databases for radiation transport studies. NASA technical paper 3644.

Tseng, H.K.; Pratt, R.H.; Yu, S. & Ron, A. (1978). Photoelectron angular distributions. *Phys. Rev. A*, 17, 1061-1079. ISSN: 1050-2947

Turner, J.E.; Hamm, R.N.; Wright, H.A.; Módolo, J.T. & Sordi, G.M.A.A. (1980). Monte Carlo calculation of initial energies of Compton electrons and photoelectrons in water irradiated by photons with energies up to 2 MeV. *Health Phys.*, 39, 49-55. ISSN: 0017-9078

Uehara, S.; Nikjoo, H. & Goodhead, D.T. (1992). Cross-sections for water vapour for the Monte Carlo electron track structure code from 10 eV to the MeV region. *Phys. Med. Biol.*, 37, 1841-1858. ISSN: 0031-9155.

Uehara, S. & Nikjoo, H. (2006). Monte Carlo simulation of water radiolysis for low-energy charged particles. *J. Radiat. Res.*, 47, 69-81. ISSN: 0449-3060

Watt, D.E. (1996). *Quantities for Dosimetry of Ionizing Radiations in Liquid Water*. Taylor & Francis, ISBN 0-203-21095-6, London, UK